A Path-Following Preview Controller for Autonomous Air Vehicles

Rita Cunha[*] and Duarte Antunes[†] and Pedro Gomes[‡] and Carlos Silvestre[§]

Instituto Superior Técnico, Institute for Systems and Robotics, 1049-001 Lisbon, Portugal

This paper addresses the path-following problem of steering an autonomous air vehicle along a predefined 3-D path, while tracking a desired velocity profile. The presented solution relies on the definition of a path-dependent error space to express the dynamic model of the vehicle, which exhibits a high degree of directional accuracy. The proposed methodology adopts a polytopic Linear Parameter Varying (LPV) representation with piecewise affine dependence on the parameters to accurately model the error dynamics over a wide flight-envelope. The synthesis problem is stated as a discrete-time H_2 control problem for LPV systems and solved using Linear Matrix Inequalities (LMIs). To achieve better path-following performance, a preview control technique is adopted, which amounts to introducing a feedforward term driven by future path disturbances. Implementation of the nonlinear controller is addressed within the framework of gain-scheduling control theory using the D-methodology. The effectiveness of the proposed controller is assessed in simulation using the full nonlinear model of a small-scale helicopter.

I. Introduction

Over the last decade, autonomous vehicles have been steadily growing a major topic of research. With the advent of new sensor technology and increasingly powerful computational systems, autonomous vehicles have the potential to perform high precision tasks in challenging and uncertain operation scenarios. Consider for example the case of bridge inspections, where a camera-equipped helicopter is expected to follow complex three-dimensional paths to monitor bridge pillars and deck and assess maintenance and repair requirements. This provides an important motivation for developing new high performance control algorithms.

Within the field of motion control for autonomous vehicles, the path-following approach arose as a response to the limitations of trajectory-tracking. Leading work in this area can be found in Ref. 1. In path-following, instead of tracking a time-parameterized reference, i.e., a trajectory, the vehicle is required to converge to and follow a path without temporal restrictions. Several examples show that, when compared to trajectory-tracking, path-following strategies consistently exhibit enhanced performance, with smoother convergence to the path and less demand on the control effort. In this paper, the path-following problem is addressed along the lines of the work reported in Ref. 2–4, while having in mind high-maneuverability vehicles, such as helicopters. The presented solution relies on the definition of a path-dependent error space to express the dynamic model of the vehicle. The error vector, which the path-following controller should drive to zero, comprises velocity errors, orientation errors, and the distance to the path, defined as the distance between the vehicle's position and its orthogonal projection on the path. Due to a more accurate representation of error directionality, the proposed error space constitutes an improvement with respect to previous ones. Namely, instead of matching the desired trimming values, the reference velocities are rotated to the current body frame. These enhancements are particularly relevant for helicopters, since the angles of attack and sideslip may change substantially while following a path.

It is well-known that LPV models used within the framework of gain-scheduling constitute a powerful tool for tackling difficult nonlinear problems. Several examples in the literature attest for its level of success (see Ref. 5,6 and references therein). In this paper, we adopt a polytopic LPV representation with piecewise affine

[*] PhD Student, Department of Electrical Engineering and Computer Science (DEEC), Av. Rovisco Pais 1; rita@isr.ist.utl.pt.

[†] PhD Student, DEEC, Av. Rovisco Pais 1; dantunes@isr.ist.utl.pt.

[‡] MSc Student, DEEC, Av. Rovisco Pais 1; pgomes@isr.ist.utl.pt.

[§] Assistant Professor, DEEC, Av. Rovisco Pais 1; cjs@isr.ist.utl.pt. Member AIAA.

dependence on the parameters to accurately model the error dynamics over a set of predefined operating regions. Using an LMI approach and based on the notion of quadratic stability for LPV systems,[7] we are able to address the path-following controller synthesis problem in a systematic way and derive in a straightforward manner a discrete-time H_2 controller for each of the operating regions.

Preview control algorithms have been widely used to improve the overall closed loop performance obtained with limited bandwidth feedback compensators when future information on the commands or disturbances is available. A series of papers on application of Linear Quadratic preview control theory to the design of vehicle active suspensions can be found in the literature. Special emphasis should be given to the pioneering work of Tomizuka,[8] where the optimal preview control problem is formulated and solved, and the impact of different preview lengths on the overall suspension performance is discussed. An alternative method is presented by Prokop and Sharp[9] that consists of incorporating the disturbance or reference dynamics into the design model and then solving the resulting linear quadratic control problem. More recently, Takaba[10] addressed the problem of robust servomechanism mixed LQ/H_∞ design with preview action for polytopic uncertain systems using Linear Matrix Inequalities. The path-following controller presented in this paper is based on the novel preview control algorithm proposed in Ref. 11 and generalizes these results to accommodate 3-D reference paths.

The paper is organized as follows: Section II presents the standard rigid-body dynamic model, which can be used to describe autonomous air vehicles; Section III introduces the path-dependent error space, presents a derivation for the error dynamics parameterized by a vector that fully characterizes the desired operating point, and particularizes for the case of helicopters, introducing a reduced parameter vector and a suitable error output vector; Section IV reviews theoretical results on LPV systems and presents a solution for the preview control problem within this framework; Section V focuses on implementation of the nonlinear path-following controller, addressing the problem of modeling the error dynamics as a set of affine parameter dependent linear systems and describing controller design specifications; simulation results obtained with the full nonlinear model of a helicopter are presented in Section VI.

II. Vehicle Dynamic Model

Consider a vehicle modeled as rigid-body, define $\{I\}$ as the inertial frame and $\{B\}$ as the body frame, attached to the vehicle's center of mass. Let $({}^I\mathbf{p}_B,\ {}^I_BR) \in SE(3) \triangleq \mathbb{R}^3 \times SO(3)$ denote the configuration of $\{B\}$ with respect to $\{I\}$ and $\boldsymbol{\lambda}_B = [\phi_B\ \ \theta_B\ \ \psi_B]^T$, $\theta_B \in \,]-\pi/2, \pi/2[$, $\phi_B, \psi_B \in \mathbb{R}$ denote the Z-Y-X Euler angles, representing the orientation of $\{B\}$ relative to $\{I\}$. The rotation matrix ${}^I_BR$ and the Euler angles $\boldsymbol{\lambda}_B$ satisfy

$$\begin{aligned} {}^I_BR = R_Z(\psi_B)R_Y(\theta_B)R_X(\phi_B) &\Leftrightarrow \boldsymbol{\lambda}_B = \arg({}^I_BR) \\ &\Leftrightarrow \begin{cases} \theta_B &= \operatorname{atan2}(-r_{31}, \sqrt{r_{11}^2 + r_{21}^2}) \\ \phi_B &= \operatorname{atan2}(r_{32}, r_{33}) \\ \psi_B &= \operatorname{atan2}(r_{21}, r_{11}) \end{cases}, \end{aligned} \tag{1}$$

where atan2(.,.) denotes the four quadrant arctangent function and $R_Z(.)$, $R_Y(.)$, and $R_X(.)$ denote rotation matrices about the Z, Y, and X axes, respectively.

Consider also the linear and angular body velocities, $\mathbf{v}_B$ and $\boldsymbol{\omega}_B \in \mathbb{R}^3$, given respectively by $\mathbf{v}_B = {}^B_IR\,{}^I\dot{\mathbf{p}}_B$ and $\boldsymbol{\omega}_B = {}^B_IR\,{}^I\boldsymbol{\omega}_B$, where ${}^I\boldsymbol{\omega}_B \in \mathbb{R}^3$ is the angular velocity of $\{B\}$ with respect to $\{I\}$. According to this notation, the standard equations for the vehicle's kinematics[12] can be written as

$$\begin{cases} {}^I\dot{\mathbf{p}}_B = {}^I_BR\,\mathbf{v}_B \\ \dot{\boldsymbol{\lambda}}_B = Q(\phi_B, \theta_B)\,\boldsymbol{\omega}_B \end{cases}, \tag{2}$$

where

$$Q(\phi_B, \theta_B) = \begin{bmatrix} 1 & \sin\phi_B \tan\theta_B & \cos\phi_B \tan\theta_B \\ 0 & \cos\phi_B & -\sin\phi_B \\ 0 & \sin\phi_B/\cos\theta_B & \cos\phi_B/\cos\theta_B \end{bmatrix}, \tag{3}$$

and the derivative of ${}^I_BR$ is given by

$${}^I_B\dot{R} = {}^I_BR\,S(\boldsymbol{\omega}_B), \tag{4}$$

where $S(x) \in \mathbb{R}^{3\times 3}$ is a skew symmetric matrix such that $S(x)\,y = x \times y$, for all $x,\, y \in \mathbb{R}^3$. The dynamic model of the vehicle can be written as

$$\begin{cases} \dot{\mathbf{v}}_B = \mathbf{f}(\mathbf{v}_B, \boldsymbol{\omega}_B, \mathbf{u}) + {}^B_I R\,[0\ 0\ g]^T \\ \dot{\boldsymbol{\omega}}_B = \mathbf{n}(\mathbf{v}_B, \boldsymbol{\omega}_B, \mathbf{u}) \end{cases}, \tag{5}$$

where g denotes the gravitational acceleration; $\mathbf{f},\, \mathbf{n} : (\mathbb{R}^3, \mathbb{R}^3, \mathbb{R}^m) \rightarrow \mathbb{R}^3$ are continuously differentiable functions of the body velocities and control inputs $\mathbf{u} \in \mathbb{R}^m$ that derive from the remaining forces and moments acting on the body.

Due to the choice of Euler angles representation, it follows that ${}^B_I R\,[0\ 0\ g]^T = R_X(\phi_B)^T R_Y(\theta_B)^T [0\ 0\ g]^T$ and so the complete dynamic model of the system can be written as

$$\begin{cases} \dot{\mathbf{v}}_B = \mathbf{f}\,(\mathbf{v}_B,\, \boldsymbol{\omega}_B,\, \mathbf{u}) + \mathbf{f}_g\,(\phi_B,\, \theta_B) \\ \dot{\boldsymbol{\omega}}_B = \mathbf{n}\,(\mathbf{v}_B,\, \boldsymbol{\omega}_B,\, \mathbf{u}) \\ {}^I\dot{\mathbf{p}}_B = {}^I_B R\, \mathbf{v}_B \\ \dot{\boldsymbol{\lambda}}_B = Q(\phi_B,\, \theta_B)\, \boldsymbol{\omega}_B \end{cases}. \tag{6}$$

III. Path-dependent Error Dynamic Model

The goal of this work consists in designing a controller that steers the vehicle along a desired path, which corresponds to a smooth three-dimensional curve Γ. In this section, we describe the transformation applied to the vehicle dynamic model (6) to obtain an error dynamic model, which will then be used for controller design. In order to define this error space, we must first introduce two coordinate frames relating the vehicle and the desired path Γ. These are the tangent frame $\{T\}$ and the desired body frame $\{C\}$ shown in Figure 1. Both coordinate frames move along the path attached to the point on the path closest to the vehicle. The difference between the two lies in the fact that $\{T\}$ is always aligned with the tangent to the path, whereas $\{C\}$ gives the desired body orientation.

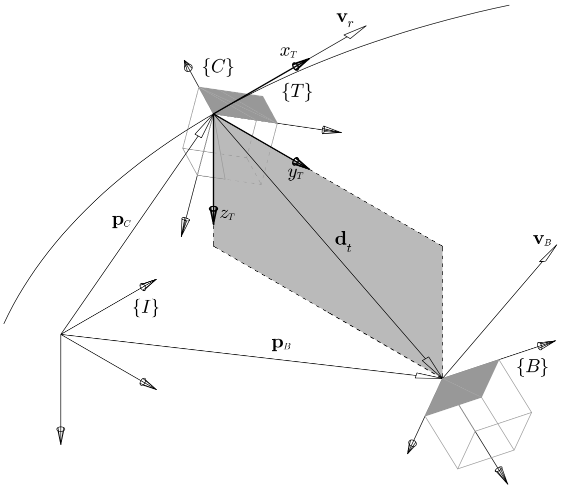

Figure 1. Coordinate frames: inertial $\{I\}$, body $\{B\}$, tangent $\{T\}$, and desired body frame $\{C\}$

A. The tangent frame $\{T\}$

There is an almost exact correspondence between $\{T\}$ and the standard Serret-Frenet frame, formed by the tangent, normal, and binormal vectors. Both frames share the same x axis, the tangent vector, and have collinear y and z axes, which may have opposite signs. In loose terms, while in the Serret-Frenet frame the normal always points "inside" the curve, this may not be case with the $\{T\}$ frame. This property widens the set of curves for which continuity in the $\{T\}$ frame can be guaranteed. To illustrate the difference between the two frame definitions, consider the sinusoidal curve depicted in Figure 2. The discontinuity in the Serret-Frenet's normal vector, shown in Figure 2(a) at the origin of the coordinate frame, is eliminated by our alternative tangent frame definition shown in Figure 2(b).

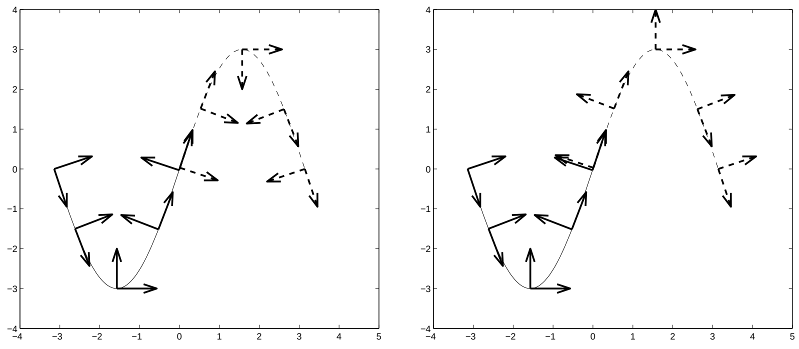

(a) Serret-Frenet frame

(b) Tangent frame

Figure 2. Sinusoidal curve

A formal definition for the $\{T\}$ coordinate frame and a derivation of the equations ruling its motion along the curve can be found in Appendix A. Assuming that the curve is parameterized by the arc-length s, also defined in Appendix A, the orientation of $\{T\}$ with respect to $\{I\}$ can be written as

$$ {}^{I}_{T}R(s) = [\mathbf{t}(s)\ \mathbf{n}(s)\ \mathbf{b}(s)] \in SO(3), \tag{7}$$

where the tangent $\mathbf{t}(s)$, the normal $\mathbf{n}(s)$, and the binormal $\mathbf{b}(s)$ are defined in (51), (55), and (56), respectively.

In the following, the dependence on s is omitted, for reasons of simplicity. Given (7), it is easy to show that *i)* since $\{T\}$ is always tangent to the path, the linear velocity $\mathbf{v}_T = {}^{T}_{I}R\,{}^{I}\dot{\mathbf{p}}_T \in \mathbb{R}^3$ takes the form

$$\mathbf{v}_T = V_T[1\ 0\ 0], \tag{8}$$

where $V_T \in \mathbb{R}$ gives the speed with which the tangent frame is moving along the curve, i.e., $V_T = \dot{s}$; *ii)* according to the Serret-Frenet formulas (59), the motion of ${}^{I}_{T}R$ is ruled by

$${}^{I}_{T}\dot{R} = \frac{\mathrm{d}({}^{I}_{T}R)}{\mathrm{d}s}\,\dot{s} = V_T\,{}^{I}_{T}R\,S([\tau\ 0\ \kappa]^T); \tag{9}$$

and *iii)* the angular velocity $\boldsymbol{\omega}_T = {}^{T}_{I}R\,{}^{I}\boldsymbol{\omega}_T$ is therefore given by

$$\boldsymbol{\omega}_T = V_T[\tau\ 0\ \kappa]^T. \tag{10}$$

Going back to the original idea of constraining the tangent frame's motion to depend on the body's motion, so that the origin of $\{T\}$ coincides with the point in Γ closest to the vehicle, it is easy to see that this condition is equivalent to restricting the distance vector $\mathbf{d} = {}^{I}\mathbf{p}_B - {}^{I}\mathbf{p}_T$ to belong to the plane perpendicular to the tangent vector $\mathbf{t}$, see Figure 1. Then, the body position relative to the path can be expressed in terms of the arc-length s and the distance vector $\mathbf{d}_t = [d_y\ d_z]^T \in \mathbb{R}^2$, which verifies

$${}^{T}_{I}R\,\mathbf{d} = [0\ \mathbf{d}_t^T]^T. \tag{11}$$

Taking the derivative of (11), it is straightforward to write

$$\begin{aligned}\begin{bmatrix}0\\ \dot{\mathbf{d}}_t\end{bmatrix} &= {}^{T}_{I}\dot{R}\,({}^{I}\mathbf{p}_B -{}^{I}\mathbf{p}_T) + {}^{T}_{I}R\,({}^{I}\dot{\mathbf{p}}_B -{}^{I}\dot{\mathbf{p}}_T)\\ &= -S\left(\boldsymbol{\omega}_T\right)\begin{bmatrix}0\\ \mathbf{d}_t\end{bmatrix} + {}^{T}_{B}R\,\mathbf{v}_B - \mathbf{v}_{\mathbf{T}}, \end{aligned}\tag{12}$$

and simple manipulations show that the speed of the tangent frame is given by

$$\dot{s} = V_T = \frac{1}{1-\kappa\,d_y}\begin{bmatrix}1 & 0 & 0\end{bmatrix}{}^{T}_{B}R\,\mathbf{v}_B \tag{13}$$

and the motion of $\mathbf{d}_t$ is ruled by

$$\dot{\mathbf{d}}_t = V_T\tau \begin{bmatrix} 0 & 1 \\ -1 & 0 \end{bmatrix} \mathbf{d}_t + \begin{bmatrix} 0 & 1 & 0 \\ 0 & 0 & 1 \end{bmatrix} {}^{T}_{B}R\,\mathbf{v}_B. \tag{14}$$

B. The desired body frame $\{C\}$

The need to define $\{C\}$ arises from the fact that while following a path, the vehicle may take different orientations or even rotate with respect to the path. The desired orientation can be represented by the Z-Y-X Euler angles $\boldsymbol{\lambda}_C = [\phi_C\ \theta_C\ \psi_C]^T$, $\theta_C \in\,]-\pi/2, \pi/2[$, $\phi_C, \psi_C \in \mathbb{R}$.

Using the tangent velocities $\mathbf{v}_T$ and $\boldsymbol{\omega}_T$, the linear and angular velocities of $\{C\}$ can be written as $\mathbf{v}_C = {}^{C}_{T}R\,\mathbf{v}_T$ and $\boldsymbol{\omega}_C = {}^{C}_{T}R\,(\boldsymbol{\omega}_T + {}^{T}\boldsymbol{\omega}_C)$, respectively, where the relative angular velocity ${}^{T}\boldsymbol{\omega}_C$ is given by $S({}^{T}\boldsymbol{\omega}_C) = V_T \frac{\mathrm{d}({}^{T}_{C}R)}{\mathrm{d}s}\,{}^{C}_{T}R$. Then, the derivative of $\boldsymbol{\lambda}_C$ can be written as

$$\dot{\boldsymbol{\lambda}}_C = Q(\phi_C, \theta_C)\,{}^{C}_{T}R\,(\boldsymbol{\omega}_T + {}^{T}\boldsymbol{\omega}_C). \tag{15}$$

C. Error space definition

In order to ensure that a vehicle not only follows a predefined curve Γ but also tracks a given velocity profile, extra references are needed. For that purpose, we consider the reference tangent speed V_r, which defines references for both the linear and angular tangent velocities given by $\mathbf{v}_r = [V_r\ 0\ 0]^T$ and $\boldsymbol{\omega}_r = V_r[\tau\ 0\ \kappa]^T$, respectively. Given the definitions of $\{T\}$, $\{C\}$, and references V_r and $\boldsymbol{\omega}_r$, we introduce the following error state vector

$$\mathbf{x}_e = \begin{bmatrix} \mathbf{v}_e \\ \boldsymbol{\omega}_e \\ \mathbf{d}_t \\ \boldsymbol{\lambda}_e \end{bmatrix} = \begin{bmatrix} \mathbf{v}_B - {}^{B}_{T}R\,\mathbf{v}_r \\ \boldsymbol{\omega}_B - {}^{B}_{T}R\,(\boldsymbol{\omega}_r + {}^{T}\boldsymbol{\omega}_C) \\ \mathbf{d}_t \\ \boldsymbol{\lambda}_B - \boldsymbol{\lambda}_C \end{bmatrix} \in \mathbb{R}^{11}. \tag{16}$$

It is now easy to see that there is a nonlinear transformation between the original vehicle state $\mathbf{x}_B = [\mathbf{v}_B^T\ \boldsymbol{\omega}_B^T\ {}^{I}\mathbf{p}_B^T\ \boldsymbol{\lambda}_C^T]^T \in \mathbb{R}^{12}$ and the state vector given by $[\mathbf{x}_e^T\ s]^T$. Moreover, it is straightforward to verify that the vehicle follows a path Γ with speed $V_T = V_r$, relative angular velocity ${}^{T}\boldsymbol{\omega}_B = {}^{T}\boldsymbol{\omega}_C$, and orientation $\boldsymbol{\lambda}_B = \boldsymbol{\lambda}_C$ if and only if $\mathbf{x}_e = 0$. It should be noted that the reference velocities are determined in the tangent frame $\{T\}$ and then rotated to the current body frame $\{B\}$. This is in contrast with previous approaches,[2] where the references were rotated to $\{C\}$ instead of $\{B\}$. With a significant orientation error, directionality of the velocity errors could be lost. In the current approach, the velocity errors $\mathbf{v}_e$ and $\boldsymbol{\omega}_e$ do not depend on the orientation error, so that keeping $\boldsymbol{\lambda}_e \neq 0$ while the remaining error components are driven to zero, still ensures that the vehicle follows the path with the desired speed, but now with arbitrary orientation. The following proposition summarizes the above considerations.

Proposition III.1. *Consider a vehicle with state $\mathbf{x}_B = [\mathbf{v}_B^T\ \boldsymbol{\omega}_B^T\ {}^{I}\mathbf{p}_B^T\ \boldsymbol{\lambda}_B^T]^T \in \mathbb{R}^{12}$, a path Γ to be followed, and the error vector $\mathbf{x}_e = [\mathbf{v}_e^T\ \boldsymbol{\omega}_e^T\ \mathbf{d}_t^T\ \boldsymbol{\lambda}_e^T]^T \in \mathbb{R}^{11}$ given by* (16)*. Then,*

(i) the vehicle follows Γ, with speed $V_T = V_r$ ($\mathbf{v}_T = \mathbf{v}_r$ and $\boldsymbol{\omega}_T = \boldsymbol{\omega}_r$) and arbitrary orientation if and only if $\mathbf{d}_t = 0$ and $\mathbf{v}_e = 0$;

(ii) the vehicle follows Γ, with speed $V_T = V_r$, relative angular velocity ${}^{T}\boldsymbol{\omega}_B = {}^{T}\boldsymbol{\omega}_C$, and arbitrary but constant orientation if and only if $\mathbf{d}_t = 0$, $\mathbf{v}_e = 0$, and $\boldsymbol{\omega}_e = 0$; and, finally,

(iii) the vehicle follows Γ, with speed $V_T = V_r$, relative angular velocity ${}^{T}\boldsymbol{\omega}_B = {}^{T}\boldsymbol{\omega}_C$, and orientation $\boldsymbol{\lambda}_B = \boldsymbol{\lambda}_C$ if and only if $\mathbf{x}_e = 0$.

Proof. i) Having the vehicle on the path is obviously equivalent to having $\mathbf{d}_t = 0$, which implies, by (13-14), that $\mathbf{v}_B = {}^{B}_{T}R\mathbf{v}_T$. Therefore,

$$\mathbf{v}_e = 0 \Leftrightarrow \mathbf{v}_B = {}^{B}_{T}R\,[V_r\ 0\ 0]^T \Leftrightarrow V_T = V_r \Leftrightarrow \boldsymbol{\omega}_T = \boldsymbol{\omega}_r,$$

ii) If $\mathbf{d}_t = 0$ and $\mathbf{v}_e = 0$ then

$$\boldsymbol{\omega}_e = 0 \Leftrightarrow \boldsymbol{\omega}_B = {}^{B}_{T}R(\boldsymbol{\omega}_r + {}^{r}\boldsymbol{\omega}_C) \Leftrightarrow {}^{B}_{T}R(\boldsymbol{\omega}_T + {}^{T}\boldsymbol{\omega}_B) = {}^{B}_{T}R(\boldsymbol{\omega}_T + {}^{T}\boldsymbol{\omega}_C) \Leftrightarrow {}^{T}\boldsymbol{\omega}_B = {}^{T}\boldsymbol{\omega}_C.$$

The proof of *iii)* follows immediately. □

D. Error Dynamics

Taking the time derivative of (16) and substituting $\dot{\mathbf{v}}_B$ and $\dot{\boldsymbol{\omega}}_B$ by the corresponding expressions given in (5) yields

$$\begin{cases} \dot{\mathbf{v}}_e = \mathbf{f}\,(\mathbf{v}_B,\, \boldsymbol{\omega}_B,\, \mathbf{u}) + \mathbf{f}_g\,(\phi_B,\, \theta_B) + S(\boldsymbol{\omega}_B - {}^B_T R\ \boldsymbol{\omega}_T)\,{}^B_T R\,\mathbf{v}_r - {}^B_T R\ \dot{\mathbf{v}}_r \\ \dot{\boldsymbol{\omega}}_e = \mathbf{n}\,(\mathbf{v}_B,\, \boldsymbol{\omega}_B,\, \mathbf{u}) + S(\boldsymbol{\omega}_B - {}^B_T R\ \boldsymbol{\omega}_T)\ {}^B_T R\,(\boldsymbol{\omega}_r + {}^T\boldsymbol{\omega}_C) - {}^B_T R\,(\dot{\boldsymbol{\omega}}_r + {}^T\dot{\boldsymbol{\omega}}_C) \\ \dot{\mathbf{d}}_t = V_T\tau \begin{bmatrix} 0 & 1 \\ -1 & 0 \end{bmatrix} \mathbf{d}_t + \begin{bmatrix} 0 & 1 & 0 \\ 0 & 0 & 1 \end{bmatrix} {}^T_B R\,\mathbf{v}_e \\ \dot{\boldsymbol{\lambda}}_e = Q(\phi_B,\, \theta_B)\boldsymbol{\omega}_B - Q(\phi_C, \theta_C)\,{}^C_T R\,(\boldsymbol{\omega}_T + {}^T\boldsymbol{\omega}_C) \end{cases} . \tag{17}$$

Recalling that V_r, κ, τ, ${}^I_T R$, and ${}^I_C R$ can be parameterized by s, the error dynamics (17) can be written in compact form as $\dot{\mathbf{x}}_e = \mathbf{f}_e(\mathbf{x}_e, s, \mathbf{u})$. The time derivative of s given in (13) can also be written in similar form and therefore the full system dynamics are described by

$$\begin{cases} \dot{\mathbf{x}}_e = \mathbf{f}_e(\mathbf{x}_e, s, \mathbf{u}) \\ \dot{s} = \mathbf{f}_s(\mathbf{x}_e, s) \end{cases} . \tag{18}$$

Until now, it has been assumed that Γ can be any smooth 3-D space curve to be followed with arbitrary velocity and orientation, provided these are continuously differentiable functions of s. The set of allowable paths is now restricted to the set of trimming paths. Similarly, the reference speed V_r and the motion of $\{C\}$ are constrained to correspond to trimming trajectories consistent with the chosen path. A trimming path corresponds to a curve that the vehicle can follow while satisfying the trimming condition, which is equivalent to having $\dot{\mathbf{v}}_B = 0$, $\dot{\boldsymbol{\omega}}_B = 0$, and $\dot{\mathbf{u}} = 0$ in (5). It is well known that, for a vehicle with dynamics described by (5) and assuming constant gravitational acceleration, the set of trimming trajectories comprises all z-aligned helices ($\dot{\kappa} = 0$, $\dot{\tau} = 0$, $\boldsymbol{\lambda}_T = [0\ \theta_T\ \psi_T]^T$, and $\dot{\boldsymbol{\lambda}}_T = \operatorname{sign}(\kappa) V_T \sqrt{\kappa^2 + \tau^2}\,[0\ 0\ 1]^T$), followed at constant speed ($\dot{V}_T = 0$) and constant orientation relative to the path (${}^T\boldsymbol{\omega}_C = 0$). For helices, the flight path angle θ_T is given by $\theta_T = \arctan(-\tau/\kappa)$, while in the case of straight lines ($\kappa = 0$, $\tau = 0$), θ_T is a predefined constant. The following set of constraints can therefore be imposed on the reference path and velocities: $\dot{V}_r = 0$, $\dot{\kappa} = 0$, $\dot{\tau} = 0$, ${}^T\boldsymbol{\omega}_C = 0$, and $\dot{\boldsymbol{\lambda}}_C = \dot{\boldsymbol{\lambda}}_T = \operatorname{sign}(\kappa) V_T \sqrt{\kappa^2 + \tau^2}\,[0\ 0\ 1]^T$.

Under these constraints, the error dynamics are given by

$$\begin{cases} \dot{\mathbf{v}}_e = \mathbf{f}\,(\mathbf{v}_B,\, \boldsymbol{\omega}_B,\, \mathbf{u}) + \mathbf{f}_g\,(\phi_B,\, \theta_B) + S(\boldsymbol{\omega}_e)\,{}^B_T R\,\mathbf{v}_r + (1 - \dfrac{V_T}{V_r})\,{}^B_T R\,S(\boldsymbol{\omega}_r)\mathbf{v}_r \\ \dot{\boldsymbol{\omega}}_e = \mathbf{n}\,(\mathbf{v}_B,\, \boldsymbol{\omega}_B,\, \mathbf{u}) + S(\boldsymbol{\omega}_e)\ {}^B_T R\ \boldsymbol{\omega}_r \\ \dot{\mathbf{d}}_t = V_T\tau \begin{bmatrix} 0 & 1 \\ -1 & 0 \end{bmatrix} \mathbf{d}_t + \begin{bmatrix} 0 & 1 & 0 \\ 0 & 0 & 1 \end{bmatrix} {}^T_B R\,\mathbf{v}_e \\ \dot{\boldsymbol{\lambda}}_e = Q(\phi_B,\, \theta_B)\boldsymbol{\omega}_B - \operatorname{sign}(\kappa) V_T \sqrt{\kappa^2 + \tau^2}\,[0\ 0\ 1]^T \end{cases} . \tag{19}$$

Notice that the rotation matrix ${}^T_B R$ can be written as ${}^T_B R = R_y(\theta_T)^T R_z(\psi_{ct} + \psi_e) R_y(\theta_B) R_x(\phi_B)$, where ψ_{ct} denotes the constant difference $\psi_C - \psi_T$. Thus, the only terms in (19) that depend explicitly on s, ψ_T and ψ_C, do not appear isolated and consequently the need to include the arc-length s in the state vector has been eliminated.

Consider the constant parameter vector $\boldsymbol{\eta} = (V_r,\, \dot{\psi}_r,\, \theta_T,\, \psi_{ct},\, \phi_C,\, \theta_C)$, where $\dot{\psi}_r = V_r\sqrt{\kappa^2 + \tau^2}$ denotes the reference yaw rate. It is easy to verify that, apart from a translation or a z-axis rotation, $\boldsymbol{\eta}$ completely characterizes a trimming trajectory. Then, as opposed to (18), the error system can be considered separately from the state s as given by

$$\dot{\mathbf{x}}_e = \bar{\mathbf{f}}_e(\mathbf{x}_e, \boldsymbol{\eta}, \mathbf{u}). \tag{20}$$

The following result shows that, for every trimming trajectory that is feasible for the vehicle in question, (20) has an equilibrium point at the origin and therefore its linearization about that point is time-invariant.

Proposition III.2. *Consider a reference vector* $\boldsymbol{\eta} = (V_r,\, \dot{\psi}_r,\, \theta_T,\, \psi_{ct},\, \phi_C,\, \theta_C)$ *that parameterizes a trimming trajectory. If there exists a constant input vector* $\mathbf{u}_\eta$ *such that*

$$\begin{cases} \mathbf{f}(\,{}^C_T R\ \mathbf{v}_r,\ {}^C_T R\ \boldsymbol{\omega}_r,\ \mathbf{u}_\eta) + \mathbf{f}_g(\phi_C, \theta_C) = 0 \\ \mathbf{n}(\,{}^C_T R\ \mathbf{v}_r,\ {}^C_T R\ \boldsymbol{\omega}_r,\ \mathbf{u}_\eta) = 0 \end{cases} , \tag{21}$$

then $\mathbf{x}_e = 0$ *is an equilibrium point of the error system* (20).

Proof. The proof follows from direct substitutions of the equilibrium point in the appropriate equations. If $\mathbf{x}_e = 0$, then by (16) $\mathbf{v}_B = {}^C_T R\, \mathbf{v}_r$, $\boldsymbol{\omega}_B = {}^C_T R\, \boldsymbol{\omega}_r$, and $\boldsymbol{\lambda}_B = \boldsymbol{\lambda}_C$, and by (13) $V_T = V_r$. Given the definition of $\mathbf{u}_\eta$, it follows that $\dot{\mathbf{v}}_B = 0$ and $\dot{\boldsymbol{\omega}}_B = 0$. Using these results in (19) yields $\dot{\mathbf{v}}_e = 0$, $\dot{\boldsymbol{\omega}}_e = 0$, $\dot{\mathbf{d}}_t = 0$ and $\dot{\boldsymbol{\lambda}}_e = Q(\phi_C,\, \theta_C)\, {}^C_T R\, \boldsymbol{\omega}_r - \operatorname{sign}(\kappa) V_r \sqrt{\kappa^2 + \tau^2}[0\ 0\ 1]^T$. Simple algebraic manipulations show that $\dot{\boldsymbol{\lambda}}_e = 0$. □

E. Example: error dynamics for model-scale helicopters

Using the error space defined in the preceding section, it is straightforward to obtain a linearization of the system about any predefined operating point. If the vehicle under consideration is fully actuated, then the set of operating points can be parameterized by $\boldsymbol{\eta}$. Otherwise, we need to define a suitable parameterization of lower dimension. In this paper, we consider the case of model-scale helicopters, which typically have four actuators forming the input vector

$$\mathbf{u} = [\theta_0\ \theta_{1c}\ \theta_{1s}\ \theta_{0t}]^T \in \mathbb{R}^4, \tag{22}$$

where θ_0 is the main rotor collective input, θ_{1c} and θ_{1s} the cyclic inputs for main rotor and Bell-Hiller flybar, and θ_{0t} the tail rotor collective input. It is easy to see that, due to the tail rotor actuation, helicopters can describe trimming trajectories with arbitrary but constant yaw angle relative to the path, that is, with arbitrary ψ_{ct}. However, the roll and pitch angles ϕ_C and θ_C are automatically constrained by this choice. These considerations suggest that the first four elements of $\boldsymbol{\eta}$, which we now denote by $\boldsymbol{\xi} = (V_r,\, \dot{\psi}_r,\, \theta_T,\, \psi_{ct})$, adequately parameterize the operating points of a helicopter over its flight envelope. We would also like to stress that due to the use of the D-methodology[17] in the final implementation scheme, the need to supply values for ϕ_C and θ_C is eliminated and therefore the problem of determining the exact vehicle orientation for each trimming condition is bypassed.

We are also interested in defining an output to be driven to zero at steady-state by means of integral action. Once again, we need to take into account the characteristic of the vehicle when defining this output. For the case of helicopters, we propose the following function

$$\mathbf{y}_e = \begin{bmatrix} \mathbf{v}_e + {}^B_T R \begin{bmatrix} 0 \\ \mathbf{d}_t \end{bmatrix} \\ \psi_e \end{bmatrix} \in \mathbb{R}^4. \tag{23}$$

The first element of $\mathbf{y}_e$, which can also be written as $\mathbf{v}_B - {}^B_T R\, [V_r\ \ -\mathbf{d}_t^T]^T$, effectively defines a new desired velocity that points towards the path as a function of $\mathbf{d}_t$. In addition, it has the advantage of expressing the distance in the current body frame.

To summarize the foregoing considerations, the error system for a helicopter can be described as

$$\mathcal{P}(\boldsymbol{\xi}) := \begin{cases} \dot{\mathbf{x}}_e = \bar{\mathbf{f}}_e(\mathbf{x}_e, \boldsymbol{\xi}, \mathbf{u}) \\ \mathbf{y}_e = \mathbf{g}(\mathbf{x}_e, \boldsymbol{\xi}) \end{cases}, \tag{24}$$

where, with an obvious abuse of notation, $\bar{\mathbf{f}}_e(\mathbf{x}_e, \boldsymbol{\xi}, \mathbf{u})$ corresponds to $\bar{\mathbf{f}}_e(\mathbf{x}_e, \boldsymbol{\eta}, \mathbf{u})$ as defined in (20) and $\mathbf{g}(\mathbf{x}_e, \boldsymbol{\xi})$ is given by (23). Recalling that $\boldsymbol{\xi}$ is a constant parameter vector, the linearization of $\mathcal{P}(\boldsymbol{\xi})$ about $(\mathbf{x}_e = 0,\, \mathbf{u} = \mathbf{u}_\xi)$ results in a time-invariant system of the form

$$\mathcal{P}_l(\boldsymbol{\xi}) = \begin{cases} \delta\dot{\mathbf{x}}_e = A_e(\boldsymbol{\xi})\delta\mathbf{x}_e + B_e(\boldsymbol{\xi})\delta\mathbf{u} \\ \delta\mathbf{y}_e = C_e(\boldsymbol{\xi})\delta\mathbf{x}_e \end{cases}, \tag{25}$$

where $A_e(\boldsymbol{\xi}) = \dfrac{\partial \bar{\mathbf{f}}_e}{\partial \mathbf{x}_e}(0, \mathbf{u}_\xi, \boldsymbol{\xi})$, $B_e(\boldsymbol{\xi}) = \dfrac{\partial \bar{\mathbf{f}}_e}{\partial \mathbf{u}}(0, \mathbf{u}_\xi, \boldsymbol{\xi})$, and $C_e(\boldsymbol{\xi}) = \dfrac{\partial \mathbf{g}}{\partial \mathbf{x}_e}(0, \boldsymbol{\xi})$. Analytical expressions for these Jacobians matrices can be found in Appendix B.

IV. Controller Synthesis

In the preceding section, we have derived a linear parameter-dependent representation for the nonlinear error system. In this section, we consider a discrete-time Linear Parameter Varying (LPV) system as a starting point and describe the control synthesis methodology adopted to design an H_2 state-feedback controller for this model. The connection with the underlying error model is presented in Section V.

A. Theoretical Background

Consider an LPV system of the form

$$\begin{cases} \mathbf{x}(k+1) = A(\boldsymbol{\xi})\mathbf{x}(k) + B_w(\boldsymbol{\xi})\mathbf{w}(k) + B(\boldsymbol{\xi})\mathbf{u}(k) \\ \quad\mathbf{z}(k) = C_z(\boldsymbol{\xi})\mathbf{x}(k) + E(\boldsymbol{\xi})\mathbf{u}(k) \end{cases}, \tag{26}$$

where $\mathbf{x}$ is the state, $\mathbf{u}$ is the control input, $\mathbf{z}$ denotes the error signal to be controlled, and $\mathbf{w}$ denotes the exogenous input signal, which includes reference commands and disturbances. The system is parameterized by $\boldsymbol{\xi}$, which is a possibly time-varying parameter vector and belongs to the set Ξ.

To analyze these systems, the useful notion of quadratic stability has been introduced (see, for example, Ref. 7).

Definition IV.1 (Quadratic Stability)**.** The system $\mathbf{x}(k+1) = A(\boldsymbol{\xi})\mathbf{x}(k)$ is said to be quadratically stable if there exists a matrix $P > 0$ such that the LMI $A(\boldsymbol{\xi})^T PA(\boldsymbol{\xi}) - P < 0$ is satisfied, for all $\boldsymbol{\xi} \in \Xi$.

It is straightforward to verify that quadratic stability is a sufficient condition for stability. Of course that without further assumptions, testing for quadratic stability involves an infinite number of LMI's. Several different structures for the LPV system have been proposed, which reduce the problem to that of solving a finite number of LMI's. In this paper, we have adopted the polytopic description, which can be used to model a wide spectrum of systems and, as shown in the next section, is an adequate choice for the system at hand.

Definition IV.2 (Polytopic LPV system)**.** The LPV system (26) is said to be polytopic if, for all $\boldsymbol{\xi} \in \Xi$, the system matrix $S(\boldsymbol{\xi}) = \begin{bmatrix} A(\boldsymbol{\xi}) & B_w(\boldsymbol{\xi}) & B(\boldsymbol{\xi}) \\ C_z(\boldsymbol{\xi}) & 0 & E(\boldsymbol{\xi}) \end{bmatrix}$ verifies $S(\boldsymbol{\xi}) \in \mathrm{co}(S_1, \dots, S_r)$, where co(.) denotes the convex hull operator and $S_i = \begin{bmatrix} A_i & B_{w_i} & B_i \\ C_{z_i} & 0 & E_i \end{bmatrix}$, for all $i \in \{1, \dots, r\}$.

According to Definition IV.2, $S(\boldsymbol{\xi})$ belongs to the polytope of matrices whose vertices correspond to the fixed systems S_1, S_2,…, S_r. If, in addition, the set Ξ is assumed to be a polytope defined as $\Xi = \mathrm{co}(\Xi_0)$, where $\Xi_0 = \{\boldsymbol{\xi}_1, \dots, \boldsymbol{\xi}_r\}$, and the dependence of $S(\boldsymbol{\xi})$ on $\boldsymbol{\xi}$ is assumed to be affine, then $S(\boldsymbol{\xi})$ satisfies

$$S(\boldsymbol{\xi}) = S\left(\sum_{i=1}^{r} \alpha_i \boldsymbol{\xi}_i\right) = \sum_{i=1}^{r} \alpha_i S(\boldsymbol{\xi}_i), \tag{27}$$

with $\sum_{i=1}^{r} \alpha_i = 1$ and $\alpha_i \in [0,\, 1]$. It follows that the vertices S_i of the matrix polytope can be identified with the vertices $\boldsymbol{\xi}_i$ of the parameter polytope, so that $S_i = S(\boldsymbol{\xi}_i)$, $i \in \{1, \dots, r\}$. The polytopic structure provides a powerful set of results when used in conjunction with the following lemma.

Lemma IV.1. [13] *Let $f : \Xi \to \mathbb{R}$ be a convex function defined on the convex set $\Xi = \mathrm{co}\{\Xi_0\}$. Then $f(\boldsymbol{\xi}) \le \gamma$, for all $\boldsymbol{\xi} \in \Xi$, if and only if $f(\boldsymbol{\xi}) \le \gamma$, for all $\boldsymbol{\xi} \in \Xi_0$.*

This result allows not only for the test of quadratic stability but also for the evaluation of a whole range of performance measures by simply considering a finite number of LMI's. In this paper, we are interested in finding a solution to the discrete-time state feedback H_2 synthesis problem. Consider the static state feedback law given by

$$\mathbf{u}(k) = K\mathbf{x}(k), \tag{28}$$

and let $\mathrm{T}_{\mathbf{zw}}$ denote the closed loop operator from $\mathbf{w}$ to $\mathbf{z}$ resulting from the interconnection of (26) and (28). Then, the H_2 synthesis problem can be described as that of finding a control matrix K that stabilizes the closed-loop system and guarantees that the H_2 norm of $\mathrm{T}_{\mathbf{zw}}$, $\|\mathrm{T}_{\mathbf{zw}}\|_2$, is smaller than a desired bound γ.

The technique used for controller design relies on results available in Ref. 14 and Ref. 13, the most important of which are summarized below after being rewritten for the case of polytopic LPV systems. In the following, $\mathrm{tr}(L)$, $\mathrm{im}(L)$, and $\ker(L)$ denote the trace, image, and kernel of matrix L, respectively.

Lemma IV.2. *A static state feedback controller guarantees the γ upper-bound for the discrete time H_2 norm of the closed loop operator $\mathrm{T}_{\mathbf{zw}}(\boldsymbol{\xi})$ with $\boldsymbol{\xi} \in \Xi$, that is,*

$$\|\mathrm{T}_{\mathbf{zw}}(\boldsymbol{\xi})\|_2 = \|(C_z(\boldsymbol{\xi}) + E(\boldsymbol{\xi})K)\big(zI - A(\boldsymbol{\xi}) - B(\boldsymbol{\xi})K\big)^{-1} B_w(\boldsymbol{\xi})\|_2 < \gamma, \ \forall \boldsymbol{\xi} \in \Xi \tag{29}$$

if and only if there are real matrices $P = P^T > 0$, K and Z such that, for all $i \in \{1, \ldots, r\}$, the following LMI system is satisfied

$$\begin{bmatrix} -P^{-1} & (A_i + B_i K) & 0 \\ (A_i + B_i K)^T & -P & (C_{z_i} + E_i K)^T \\ 0 & (C_{z_i} + E_i K) & -I \end{bmatrix} < 0 \tag{30}$$

$$\begin{bmatrix} P^{-1} & B_{w_i} \\ B_{w_i}^T & Z \end{bmatrix} > 0 \tag{31}$$

$$\mathrm{tr}(Z) < \gamma^2. \tag{32}$$

The synthesis problem, i.e. that of finding a matrix $P = X^{-1}$ and controller K that verify (30-32), can be solved according to the following result.

Lemma IV.3. *The H_2 norm of the closed loop operator $\mathrm{T}_{\mathbf{zw}}(\boldsymbol{\xi})$ is less than a positive number γ, that is, $\|\mathrm{T}_{\mathbf{zw}}(\boldsymbol{\xi})\|_2 < \gamma$, with $\boldsymbol{\xi} \in \Xi$ if, for all $i \in \{1, \ldots, r\}$, a real symmetric matrix $X > 0$ ($X = P^{-1}$) and a real matrix Z exist such that*

$$(W_{1_i}^T A_i + W_{2_i}^T C_{z_i}) X (W_{1_i}^T A_i + W_{2_i}^T C_{z_i})^T - W_{1_i}^T X W_{1_i} - W_{2_i}^T W_{2_i} < 0 \tag{33}$$

$$\begin{bmatrix} X & B_{w_i} \\ B_{w_i}^T & Z \end{bmatrix} > 0 \tag{34}$$

$$\mathrm{tr}(Z) < \gamma^2, \tag{35}$$

where matrices $W_{1_i}^T$ and $W_{2_i}^T$ satisfy $\mathrm{im}[W_{1_i}^T \ W_{2_i}^T]^T = \ker[B_i^T \ E_i^T]$. Using the matrix solution X, the static state feedback gain K is then computed by solving the following LMI feasibility problem:

$$\begin{bmatrix} -X & A_i & 0 \\ A_i^T & -X^{-1} & C_{z_i}^T \\ 0 & C_{z_i} & -I \end{bmatrix} + \begin{bmatrix} B_i \\ 0 \\ E_i \end{bmatrix} K [0 \ I \ 0] + \begin{bmatrix} 0 \\ I \\ 0 \end{bmatrix} K^T [B_i^T \ 0 \ E_i^T] < 0. \tag{36}$$

This result can be easily proven by using the Projection Lemma,[14] followed by a decomposition of the null space matrices. Finally, the optimal solution for the discrete time H_2 control problem is approximated through the minimization of γ subject to Lemma IV.3.

B. Discrete-Time Preview Control

Better path-following performance with limited bandwidth compensators can be achieved by taking into account, in the control law, the characteristics of the reference path ahead of the vehicle. The technique used in this paper to develop a path-following controller generalizes the results presented in Ref. 11, and amounts to introducing a dynamic feedforward block fed by future path disturbances. We recall that, in this section, we consider a general LPV system and defer to the next section the presentation of the method adopted to model the path-following error dynamics as such.

Consider an LPV system of the form (26) that depends affinely on the parameter vector $\boldsymbol{\xi} \in \Xi = \mathrm{co}(\Xi_0)$ and assume that there is an extra exogenous input $\mathbf{s}$ for which future samples can be previewed, i.e. rewrite the state equation in (26) as

$$\mathbf{x}(k+1) = A(\boldsymbol{\xi})\mathbf{x}(k) + B_w(\boldsymbol{\xi})\mathbf{w}(k) + B(\boldsymbol{\xi})\mathbf{u}(k) + B_1(\boldsymbol{\xi})\mathbf{s}(k).$$

Assuming a preview length of p samples, let $\mathbf{x}_s(k) = [\mathbf{s}(k)^T, \mathbf{s}(k+1)^T, ..., \mathbf{s}(k+p)^T]^T \in \mathbb{R}^{(s(p+1))\times 1}$ be the vector containing all the preview inputs at instant k. We are interested in determining the control matrices K_d and K_s for a controller of the form

$$\mathbf{x}_s(k+1) = D\mathbf{x}_s(k) + B_s \mathbf{s}(k+p+1) \tag{37}$$

where

$$D = \begin{bmatrix} 0 & I & 0 & \cdots & 0 \\ 0 & 0 & I & \cdots & 0 \\ \vdots & \vdots & \ddots & \ddots & \vdots \\ 0 & 0 & 0 & \ddots & I \\ 0 & 0 & 0 & \cdots & 0 \end{bmatrix}, \quad B_s = \begin{bmatrix} 0 \\ 0 \\ \vdots \\ 0 \\ I \end{bmatrix},$$

and the augmented system with state $\bar{\mathbf{x}}(k) = \begin{bmatrix}\mathbf{x}(k)^T \mathbf{x}_s(k)^T\end{bmatrix}^T$ can be written as

$$\begin{cases} \bar{\mathbf{x}}(k+1) = \bar{A}(\boldsymbol{\xi})\mathbf{x}(k) + \bar{B}(\boldsymbol{\xi})\mathbf{u}(k) + \bar{B}_w(\boldsymbol{\xi})\mathbf{w}(k) + \bar{B}_s\mathbf{s}(k+p+1) \\ \bar{\mathbf{z}}(k) = \bar{C}_z(\boldsymbol{\xi})\mathbf{x}(k) + \bar{E}(\boldsymbol{\xi})\mathbf{u}(k) \end{cases}, \tag{38}$$

where

$$\bar{A}(\boldsymbol{\xi}) = \begin{bmatrix} A(\boldsymbol{\xi}) & H(\boldsymbol{\xi}) \\ 0 & D \end{bmatrix}, \ \bar{B}(\boldsymbol{\xi}) = \begin{bmatrix} B(\boldsymbol{\xi}) \\ 0 \end{bmatrix}, \bar{B}_w(\boldsymbol{\xi}) = \begin{bmatrix} B_w(\boldsymbol{\xi}) \\ 0 \end{bmatrix}, \ \bar{B}_s = \begin{bmatrix} 0 \\ B_s \end{bmatrix},$$

the matrices $\bar{C}_z(\boldsymbol{\xi})$ and $\bar{E}(\boldsymbol{\xi})$ determine a new output signal $\bar{\mathbf{z}}$ that incorporates $\mathbf{z}$, and $H(\boldsymbol{\xi}) = \begin{bmatrix} B_1(\boldsymbol{\xi}) & 0 & \cdots & 0 \end{bmatrix}$ has as its first element the injection matrix for $\mathbf{s}(k)$ on the original system. Recalling that we are interested in determining a state-feedback controller, which can be written as

$$\mathbf{u}(k) = K_d\mathbf{x}(k) + K_s\mathbf{x}_s,$$

and noting that D is a stable matrix, it is straightforward to observe that the stability of the resulting closed-loop system is determined exclusively by K_d.

In this paper, we adopt the design methodology described in Ref. 15, which consists of *i)* designing K_d to minimize the H_2 norm of the LPV system without preview and *ii)* computing K_s to meet specific performance criteria for the system evaluated at the central point of Ξ. We denote this point by $\boldsymbol{\xi}_o$ and the corresponding state space matrices by A_o, B_o, B_{wo}, and B_{1o}. For the sake of completeness, we state the result presented in Ref. 15, which provides the expression for K_s.

Result IV.4. *Consider the matrices* $Q = \begin{bmatrix} Q_d & Q_{ds} \\ Q_{ds}^T & Q_s \end{bmatrix} = \bar{C}_z{}^T\bar{C}_z$ *and* $R = \bar{E}^T\bar{E}$*, where* Q *is partitioned according to the structure of* (38)*. Further assume that* $\bar{C}_z^T\bar{E} = 0$*. Given a pair* $(P_d,\, K_d)$*,* $P_d = P_d^T > 0$ *that satisfies the conditions of Lemma IV.2 for the LPV system* (26)*, consider the matrix*

$$P_{ds} = [\tilde{A}_c^T P_d B_o,\, (\tilde{A}_c^2)^T P_d B_o,\, \cdots,\, (\tilde{A}_c^{p+1})^T P_d B_o] + [Q_1, \tilde{A}_c^T Q_1 + Q_2, ..., \sum_{j=1}^{p+1} (\tilde{A}_c^{p+1-j})^T Q_j], \tag{39}$$

where $\tilde{A}_c = A_o - B_o\left(B_o^T P_d B_o + R\right)^{-1} B_o^T P_d A_o$ *and* Q_j *denotes the jth s-dimensional column block of matrix* Q_{ds}*, and the matrix* P_s *with entries*

$$P_s(i,j) = \begin{cases} \Delta(i,j) & , \scriptstyle{i \leq s \,\vee\, j \leq s} \\ \Delta(i,j) + P_s(i-s, j-s) & , \scriptstyle{i > s \,\wedge\, j > s} \end{cases} \tag{40}$$

$$\Delta = H_o^T P_d H_o + H_o^T P_{ds} D + D^T P_{ds} H_o + Q_s - (P_d H_o + P_{ds} D)^T B_o (B_o^T P_d B_o + R)^{-1} B_o^T (P_d H_o + P_{ds} D).$$

Consider also the feedforward gain matrix

$$K_s = \left(B_o^T P_d B_o + R\right)^{-1} B_o^T \left(P_d H_o + P_{ds} D\right). \tag{41}$$

Then, the closed-loop system resulting from the interconnection of (26) *and* (37) *is stable over the whole region* Ξ *and the Lyapunov inequality for the central point verifies*

$$(\bar{A}_o + \bar{B}_o K)^T P (\bar{A}_o + \bar{B}_o K) - P + (\bar{C}_z + \bar{E}K)^T (\bar{C}_z + \bar{E}K) = \begin{bmatrix} \Lambda & 0 \\ 0 & 0 \end{bmatrix} \leq 0, \tag{42}$$

with $P = \begin{bmatrix} P_d & P_{ds} \\ P_{ds}^T & P_s \end{bmatrix} > 0$ *and* $K = \begin{bmatrix} K_d & K_s \end{bmatrix}$*.*

V. Implementation

A. Affine Parameter Dependent Approximation of the Error Dynamics

In this section, we bridge the gap between the results of sections III and IV by taking the path-following error dynamics and approximating it by a discrete-time polytopic LPV system with affine dependence on a given set of parameters. The forthcoming results were obtained for the nonlinear helicopter simulation model SimModHeli,[16] parameterized for a specific platform the Vario X-treme helicopter. To apply the preview methodology, we also need to introduce an additional exogenous input that takes into account discontinuities in the reference path, and therefore can be used as a preview input.

For that purpose, we recall the error space definition and assume that at time t_i there is a discontinuity in the reference path such that

$$\frac{\mathrm{d}({}^{I}_{T}R\,\mathbf{v}_r)}{\mathrm{d}t}(t_i) = {}^{I}_{T}R\,(t_i^-)\delta(0)\left({}^{T}_{I}R(t_i^-){}^{I}_{T}R(t_i^+)\mathbf{v}_r(t_i^+) - \mathbf{v}_r(t_i^-)\right) \tag{43}$$

$$\frac{\mathrm{d}({}^{I}_{T}R\,\boldsymbol{\omega}_r)}{\mathrm{d}t}(t_i) = {}^{I}_{T}R\,(t_i^-)\delta(0)\left({}^{T}_{I}R(t_i^-){}^{I}_{T}R(t_i^+)\boldsymbol{\omega}_r(t_i^+) - \boldsymbol{\omega}_r(t_i^-)\right) \tag{44}$$

$$\frac{\mathrm{d}\boldsymbol{\lambda}_C}{\mathrm{d}t}(t_i) = \delta(0)\left(\boldsymbol{\lambda}_C(t_i^+) - \boldsymbol{\lambda}_C(t_i^-)\right), \tag{45}$$

where $\delta(.)$ denotes the Dirac delta function. A detailed analysis of the error dynamics suggests the introduction of three disturbance terms due to (43), (44), and (45), so that the linearized error state equation becomes

$$\delta\dot{\mathbf{x}}_e = A_e(\boldsymbol{\xi})\delta\mathbf{x}_e + B_e(\boldsymbol{\xi})\delta\mathbf{u} + W(\boldsymbol{\xi})\delta\mathbf{w}, \tag{46}$$

with the injection matrix W given by $W(\boldsymbol{\xi}) = \begin{bmatrix} {}^{C}_{T}R(\boldsymbol{\xi}) & 0 & 0 \\ 0 & {}^{C}_{T}R(\boldsymbol{\xi}) & 0 \\ 0 & 0 & 0 \\ 0 & 0 & I \end{bmatrix}$.

The corresponding discretization can be written as

$$\mathbf{x}(k+1) = A(\boldsymbol{\xi})\mathbf{x}(k) + B(\boldsymbol{\xi})\mathbf{u}(k) + B_1(\boldsymbol{\xi})\mathbf{s}(k), \tag{47}$$

where the matrices $A = e^{A_e T}$, $B = \int_0^T e^{A_e \tau} B_e d\tau$, and $B_1 = e^{A_e T} W$ were obtained assuming a zero-order hold on the input $\mathbf{u}$ and an impulse signal on the input $\mathbf{s}$, both synchronized with the sampling time T.

To define a polytopic LPV model, we consider the parameter vector $\boldsymbol{\xi} = (V_r, \dot{\psi}_r, \theta_T, \psi_{ct})$ and partition the parameter domain into the 98 convex regions (each with 16 vertices), which result from the combination of intervals defined for each of the parameters. The values for these intervals, which are presented in Table 1, were selected to encompass a wide range of operating conditions.

Table 1. Parameter intervals for flight envelope partitioning

Parameters	Intervals	
V_r	[0 1], [0.9 1.9]	(m/s)
$\dot{\psi}_r$	[−0.2 0.2]	(rad/s)
θ_T	[−90 − 60], [−65 − 35], [−40 − 10], [−15 15], [10 40], [35 65], [60 90]	(deg)
ψ_{ct}	[−90 − 60], [−65 − 35], [−40 − 10], [−15 15], [10 40], [35 65], [60 90]	(deg)

To illustrate the shape of the operating regions obtained, Figure 3 shows 2-D representations where two parameters are free to vary and the remaining are fixed. Notice that there is overlapping between adjacent regions, which can be used to implement an hysteresis commutation between controllers.

Within each region, the state space matrices of the discrete-time system (47) were approximated by affine function of $\boldsymbol{\xi}$ using Least Squares Fitting. For a relatively dense grid of evaluated operating points, the affine approximation results in an average error in the matrix entries of less than 6.2%. Then, the resulting system was evaluated at the vertices of each region, producing the finite set of state space matrices S_i, $i \in \{1, \ldots, 16\}$, needed for control system design.

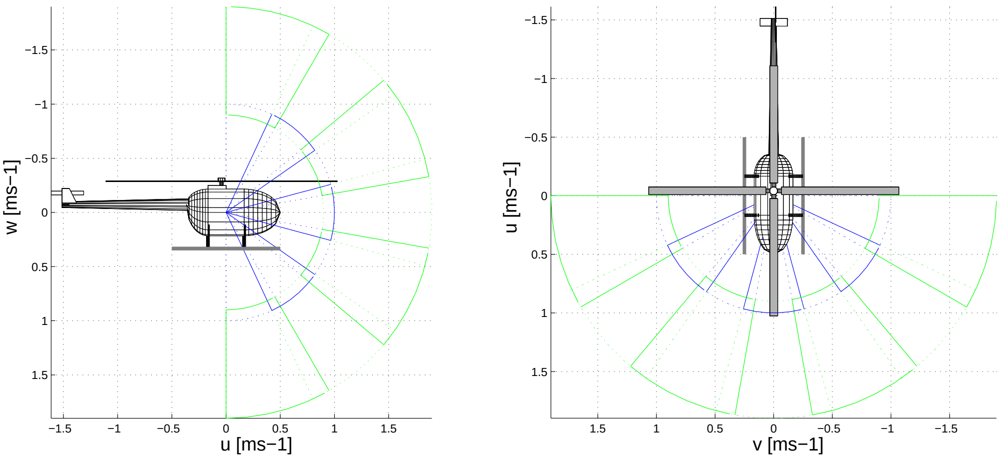

(a) *uw* plane partitioning (b) *uv* plane partitioning

Figure 3. 2-D operating regions

B. Synthesis Model and Controller Design

The linear state feedback controllers were required to meet the following design specifications:

Zero Steady State Error. Achieve zero steady state values for the error variable $\mathbf{y}_e$.

Bandwidth Requirements. The control loop bandwidth for the actuators channels should not exceed 10 rad/s ; this limit was selected to ensure that the actuators would not be driven beyond their normal actuation bandwidth.

The first step in the controller design procedure is the development of a synthesis model that can serve as an interface between the designer and the H_2 controller synthesis algorithm.

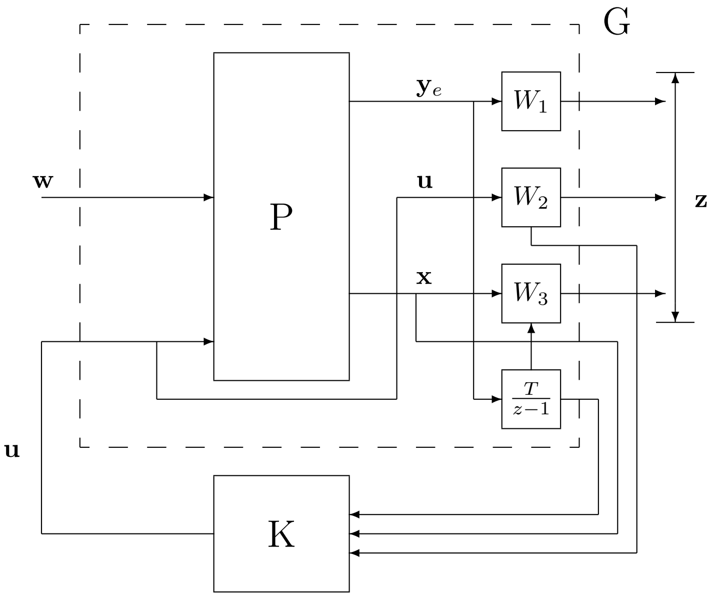

Figure 4. Synthesis model

Consider the feedback system shown in Fig. 4, where P is the discrete-time linear model of the helicopter error dynamics, and K is a state feedback controller to be designed. The augmented system G shown within the dashed line is the synthesis model, which is derived from the linear model of the plant by appending the depicted weights. In practice, the weights serve as tuning "knobs" which the designer can adjust to meet the desired performance specifications.

In the figure, $\mathbf{w}$ corresponds to the error space disturbance signals $\mathbf{s}$ that must be rejected. To meet the disturbance rejection response requirement the weighting function W_1 was chosen as $W_1 = 0.1I_4$. The weight W_2 on the actuation vector $\mathbf{u}$ was set to $W_2 = \text{diag}([W_{2a}(z)[1\ 1\ 1], W_{2b}(z)])$, where $W_{2a}(z)$ and $W_{2b}(z)$ are dynamic weights used to enforce the bandwidth constraint on the main rotor and tail rotor actuators, as discussed later. The weight W_3 was set to $W_3 = \text{diag}([0.5[1\ 1\ 1], 0.1[1\ 1\ 1], 0.01[1\ 1], 0.1])$ to meet the command bandwidth requirements. Notice the existence of a block of integrators $T/(z-1)$ that operates on the tracking errors $\mathbf{e}$. The sampling time T was set to 0.02 s.

For the case studied in this paper, the transfer functions $W_{2a}(z)$ and $W_{2b}(z)$ were set to

$$W_{2a}(z) = \frac{5.658z - 4.989}{z - 0.331} \qquad \text{and} \qquad W_{2b}(z) = \frac{1.052z + 0.3227}{z + 0.3748}.$$

The inclusion of these high-pass weights expedites the process of fine tuning the closed loop bandwidths of the control inputs because it penalizes high frequency components of the actuation signals.

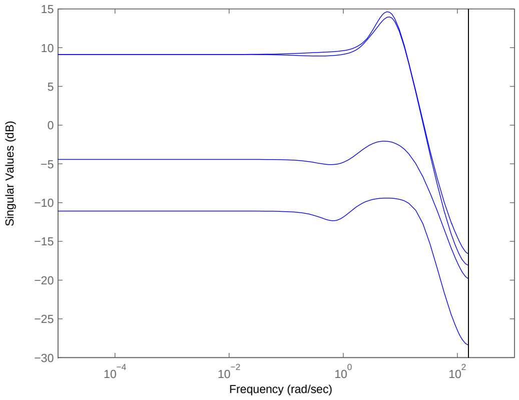

Figure 5. Closed loop frequency response

Figure 5 shows the singular value plot for the closed loop transfer functions from the input disturbance $\mathbf{s}$ to the actuation $\mathbf{u}$, for an operating point with parameters $V_r = 1.5$ m/s, $\dot{\psi}_r = 0$ rad/s, $\theta_T = 0$ rad, and $\psi_{ct} = 0$ rad. The diagram shows that the performance requirements and the actuator bandwidth constraints are met by the resulting closed loop system.

To summarize, the synthesis model G can be written as

$$\left\{\begin{array}{l} \begin{bmatrix} \mathbf{x}(k+1) \\ \mathbf{x}_i(k+1) \\ \mathbf{x}_f(k+1) \end{bmatrix} = \begin{bmatrix} A & 0 & 0 \\ TC_e & I & 0 \\ 0 & 0 & A_f \end{bmatrix} \begin{bmatrix} \mathbf{x}(k) \\ \mathbf{x}_i(k) \\ \mathbf{x}_f(k) \end{bmatrix} + \begin{bmatrix} B \\ 0 \\ B_f \end{bmatrix} \mathbf{u}(k) + \begin{bmatrix} B_w \\ 0 \\ 0 \end{bmatrix} \mathbf{w}(k) \\ \tilde{\mathbf{z}}(k) = \tilde{C}_z \begin{bmatrix} \mathbf{x}(k) \\ \mathbf{x}_i(k) \\ \mathbf{x}_f(k) \end{bmatrix} + \tilde{E}\mathbf{u}(k) \end{array}\right. , \tag{48}$$

where A_f, B_f, $\tilde{C}_z$, and $\tilde{E}$ are determined by the weights W_i, $i \in \{1, \ldots, 4\}$.

The final gain-scheduled implementation scheme, presented in Figure 6, was achieved using the D-methodology described in Ref. 17. This methodology moves all integrators to the plant input, and adds differentiators where they are needed to preserve the transfer functions and the stability characteristics of the closed loop system. The D-methodology implementation has several important features, which include the following: *i)* auto-trimming property - the controller automatically generates adequate trimming values for the actuation signals and for the state variables that are not required to track reference inputs and *ii)* the implementation of anti-windup schemes is straightforward, due to the placement of the integrators at the plant input.

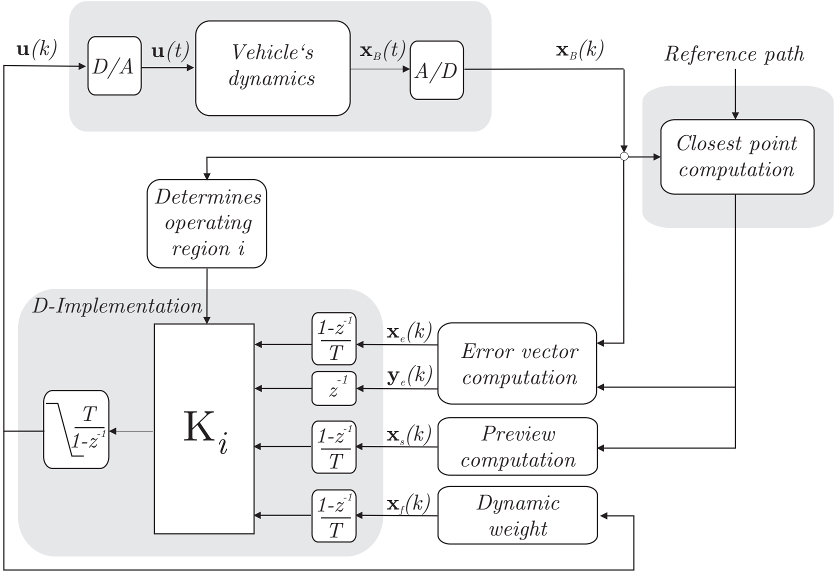

Figure 6. Implementation setup using gain scheduling and the D-methodology.

VI. Simulation Results

Simulation results were obtained using the nonlinear dynamic model *SimModHeli*, parameterized for the Vario X-Treme model-scale helicopter (see Ref. 18 for further details). In the paper we present two examples that are illustrative of the performance that can be achieved for different reference paths. Both simulations were obtained using a gain-scheduled controller with dynamic weights on the actuation, based on the linear controller synthesized for the 98 regions defined in section V.A.

The first example considers a reference path formed by the concatenation of two orthogonal straight lines to be followed at a speed of 1.5 m/s (see Figure 7). Notice that the reference transition is very abrupt and therefore could potentially drive the system to instability. The results shows that this is not the case. Moreover, comparing Figures 7(a) and (b), we can verify that the preview controller, which was designed for a preview vector with 60 samples, provides a considerable improvement in performance. The control activity and error vector evolution, depicted in Figures 8(c) and (d), respectively, clearly show that the transition is adequately anticipated by the system, due to the action of the preview term. An additional tool used to assess the performance of the preview control scheme consists of comparing the H_2 norm of the linear closed-loop systems resulting from application of the control strategies with and without preview action. Considering the whole set of operating regions, the H_2 norm for the closed-loop systems evaluated at the central point vary between 6.23 and 6.77 without preview, and are reduced to the interval between 2.36 and 2.41 when preview is applied.

For the second example, we selected a 3-D reference path divided in three segments: *i)* a climbing ramp in the *yoz* plane, *ii)* a level flight segment along the x axis, and *iii)* a climbing helix. The parameters corresponding to each stage are presented in Table 2. Notice that during the second stage, the vehicle is required to follow the path sideways. Figure 9 shows that after each transition, the helicopter quickly converges to the reference path, while keeping the actuation within the limits of operation. Notice that this avoids damaging the helicopter main rotor transmission.

Table 2. Reference path parameters

V_r(m/s)	$\dot{\psi}_r$(rad/s)	θ_T(rad)	ψ_{ct}(rad)
1.5	0	-0.46	0
1.5	0	0	$\pi/2$
1.5	0.15	-0.20	0

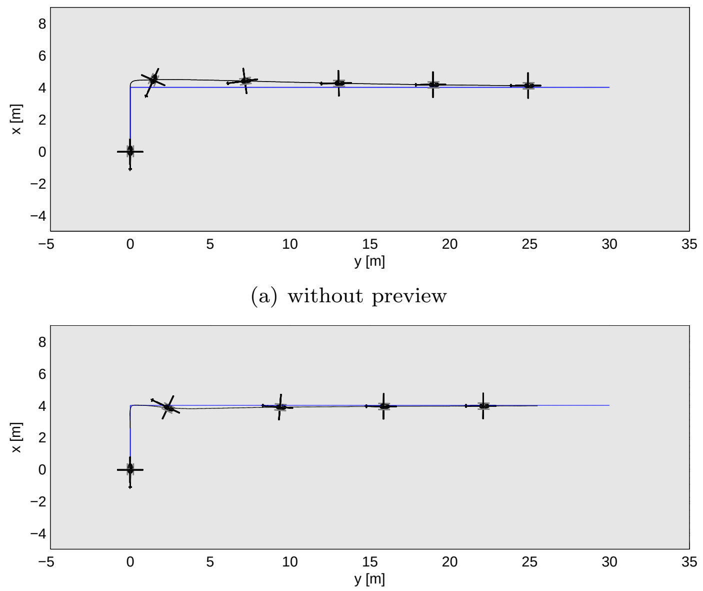

(a) without preview

(b) with preview

Figure 7. Path-following results with and without preview.

VII. Conclusions

The paper presented the design and performance evaluation of a path-following controller for autonomous air vehicles. The technique described achieves good path-following performance by taking into account, in the control law, the reference path characteristics ahead of the vehicle. An H_2 controller design methodology for polytopic LPV systems is adopted, which exploits dynamics weights to limit the actuation bandwidth. The technique presented relies on a new error space capable of naturally describing the particular dynamic characteristics of the aircraft in a suitable flight envelope. An alternative algorithm was used for computing the feed-forward gain matrix that avoids solving Linear Matrix Inequalities involving large numbers of unknowns. The resulting nonlinear controller was synthesized and implemented within the scope of gain-scheduling control theory, using a piecewise affine parameter-dependent model representation for the given set of operating regions. The effectiveness of the new control law was assessed in a simulation environment with a full nonlinear model of the Vario X-Treme helicopter. The quality of the results obtained clearly indicates that the methodology derived is suitable for the proposed application.

Appendix

A. Space Curves and the Tangent Coordinate Frame

A curve in 3-D space can be defined with respect to a parameter $\xi \in \mathbb{R}$ as the continuous map

$$\mathbf{p} : [\xi_0,\, \xi_1] \mapsto \mathbb{R}^3 : \mathbf{p}(\xi) = [x(\xi)\; y(\xi)\; z(\xi)]^T. \tag{49}$$

We are interested in smooth curves, which are twice differentiable and have nowhere zero velocity, i.e., $\frac{\mathrm{d}\mathbf{p}}{\mathrm{d}\xi}(\xi) \neq 0 \, \forall \xi \in [\xi_0,\, \xi_1]$.

The length of the curve over the domain $[\xi_0, \xi]$, also called the arc-length s, is given by

$$s(\xi) = \int_{\xi_0}^{\xi} \left\| \frac{\mathrm{d}\mathbf{p}}{\mathrm{d}\tau}(\tau) \right\| \mathrm{d}\tau. \tag{50}$$

Defining the tangent vector $\mathbf{t}(\xi)$ as

$$\mathbf{t}(\xi) = \frac{\mathrm{d}\mathbf{p}}{\mathrm{d}s}(\xi), \tag{51}$$

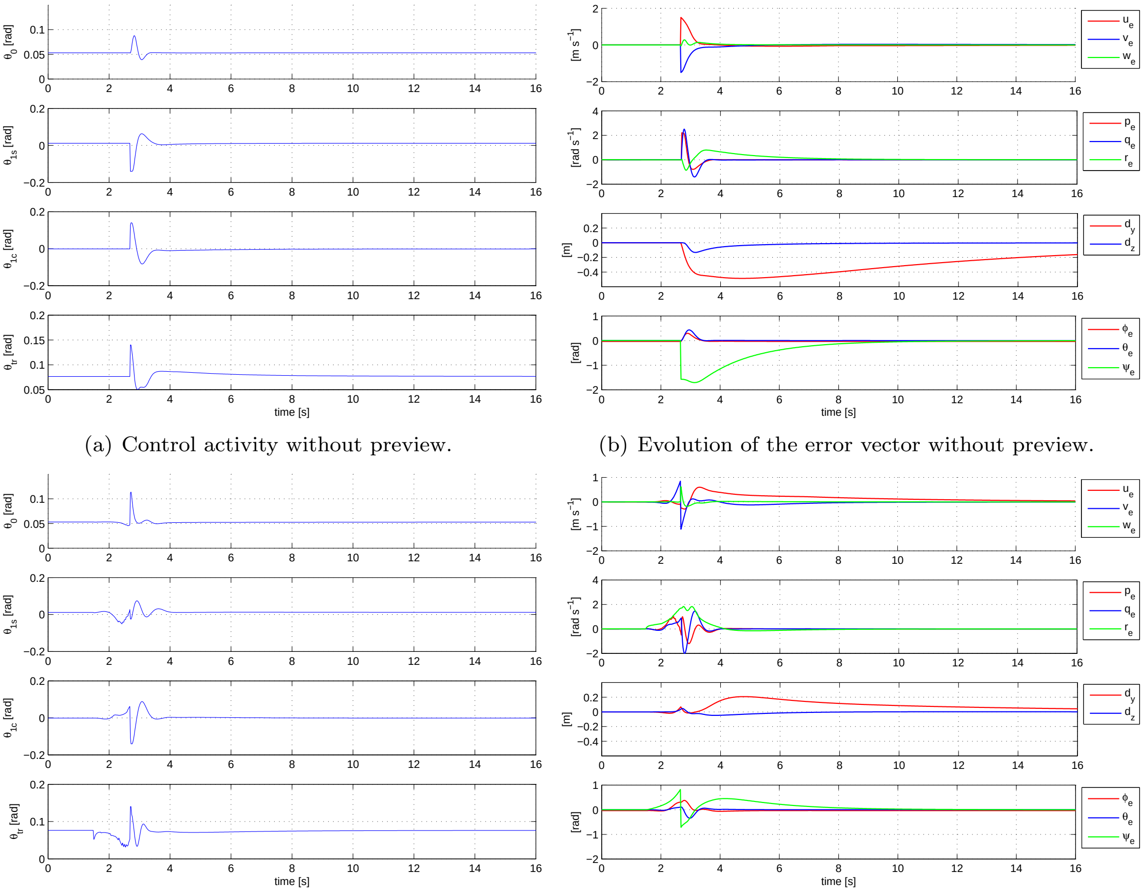

(a) Control activity without preview.

(b) Evolution of the error vector without preview.

(c) Control activity with preview.

(d) Evolution of the error vector with preview.

Figure 8. Control activity and error state with and without preview.

and noting that $\frac{d\mathbf{p}}{d\xi}(\xi) = \frac{d\mathbf{p}}{ds}(s(\xi))\frac{ds}{d\xi}(\xi)$ and $\frac{ds}{d\xi}(\xi) = \left\|\frac{d\mathbf{p}}{d\xi}(\xi)\right\|$ then $\mathbf{t}(\xi)$ can also be written as

$$\mathbf{t}(\xi) = \frac{d\mathbf{p}}{d\xi}(\xi)\left\|\frac{d\mathbf{p}}{d\xi}(\xi)\right\|^{-1}, \tag{52}$$

and therefore, we have that $\mathbf{t}$ is unitary and tangent to the curve at each point.

The normal vector is defined as satisfying

$$\frac{d\mathbf{t}}{ds}(\xi) = \kappa(\xi)\mathbf{n}(\xi), \tag{53}$$

where $\kappa(\xi) \in \mathbb{R}$ denotes what we call the “signed” curvature given by

$$\kappa(\xi) = \sigma(\xi)\left\|\frac{d\mathbf{t}}{ds}(\xi)\right\|, \quad \sigma(\xi) \in \{-1, 1\}. \tag{54}$$

Notice that (53) and (54) are not sufficient to determine $\mathbf{n}(\xi)$ when $\kappa(\xi) = 0$. We will complete this definition so as to ensure that frame $\{T\}$ is continuous along the curve. This would not be possible if instead of (54), we had considered the standard definition of curvature $\kappa(\xi) = \left\|\frac{d\mathbf{t}}{ds}(\xi)\right\|$, which is used to define the Serret-Frenet frame.

Assuming that $\kappa(\xi) = 0$ only at isolated points and given an initial value $\sigma(\xi_0)$, the map $\sigma : [\xi_0, \xi_1] \mapsto$

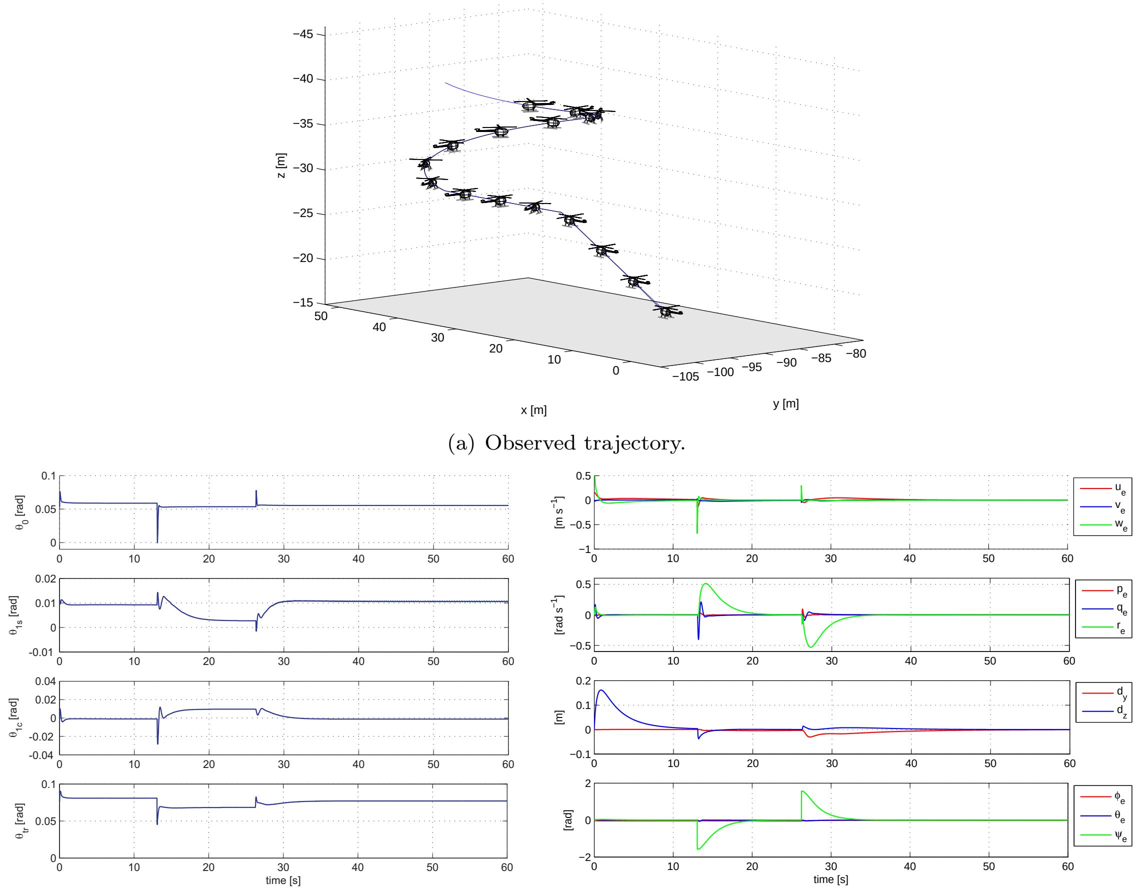

(a) Observed trajectory.

(b) Time evolution of the input vector $\mathbf{u}$.

(c) Time evolution of the error vector $\mathbf{x}_e$.

Figure 9. 3-D Path-following results.

$\{-1, 1\}$ and the normal vector $\mathbf{n}(\xi)$ can be defined as follows

$$\mathbf{n}(\xi) = \begin{cases} \dfrac{\mathrm{d}\mathbf{t}}{\mathrm{d}s}(\xi)\kappa(\xi)^{-1}, & \kappa(\xi) \neq 0 \\ \lim\limits_{\tau \to \xi^-} \mathbf{n}(\tau), & \kappa(\xi) = 0 \end{cases} \qquad \sigma(\xi) = \begin{cases} \dfrac{\mathrm{d}\sigma}{\mathrm{d}\xi}(\xi) = 0, & \kappa(\xi) \neq 0 \\ \mathbf{n}(\xi)^T \left(\lim\limits_{\tau \to \xi^+} \dfrac{\mathrm{d}\mathbf{t}}{\mathrm{d}s}(\tau) \left\| \dfrac{\mathrm{d}\mathbf{t}}{\mathrm{d}s}(\tau) \right\|^{-1} \right), & \kappa(\xi) = 0 \end{cases} \tag{55}$$

The same idea carries through to cases where $\kappa(\xi) = 0$ inside intervals. Using (54) and (55), it is easy to show that $\mathbf{n}(\xi)$ is unitary. Moreover, it can be verified that $\mathbf{t}(\xi)$ and $\mathbf{n}(\xi)$ are perpendicular by noting that $\mathbf{t}(\xi)$ is unitary and therefore $\mathbf{t}(\xi)^T \frac{\mathrm{d}\mathbf{t}}{\mathrm{d}s}(\xi) = 0$. Given these properties, $\mathbf{n}(\xi)$ can be chosen as the second axis of our tangent frame. Since we are interested in defining an orthogonal coordinate frame, the third axis, which corresponds to the binormal vector $\mathbf{b}(\xi)$, is completely determined by

$$\mathbf{b}(\xi) = \mathbf{t}(\xi) \times \mathbf{n}(\xi). \tag{56}$$

Computing the derivative of $\mathbf{b}(\xi)$ and taking the cross product with $\mathbf{n}(\xi)$, we obtain

$$\mathbf{n}(\xi) \times \frac{\mathrm{d}\mathbf{b}}{\mathrm{d}s}(\xi) = \mathbf{n}(\xi) \times \left(\mathbf{t}(\xi) \times \frac{\mathrm{d}\mathbf{n}}{\mathrm{d}s}(\xi) \right) = \left(\mathbf{t}(\xi)\mathbf{n}(\xi)^T - \mathbf{t}(\xi)^T \mathbf{n}(\xi) I_3 \right) \frac{\mathrm{d}\mathbf{n}}{\mathrm{d}s}(\xi) = 0,$$

where the results $\mathbf{n}(\xi) \times \frac{\mathrm{d}\mathbf{t}}{\mathrm{d}s}(\xi) = 0$, $\mathbf{t}(\xi)^T \mathbf{n}(\xi) = 0$, and $\mathbf{n}(\xi)^T \frac{\mathrm{d}\mathbf{n}}{\mathrm{d}s}(\xi) = 0$ were used. It follows that $\mathbf{n}(\xi)$ and $\frac{\mathrm{d}\mathbf{b}}{\mathrm{d}s}(\xi)$ are collinear and therefore can be related by the equation

$$\frac{\mathrm{d}\mathbf{b}}{\mathrm{d}s}(\xi) = -\tau(\xi)\mathbf{n}(\xi), \tag{57}$$

which defines the torsion of the curve at ξ, denoted here by $\tau(\xi) \in \mathbb{R}$. Using (53) and (57), it is straightforward to obtain

$$\frac{\mathrm{d}\mathbf{n}}{\mathrm{d}s}(\xi) = \frac{\mathrm{d}\mathbf{b}}{\mathrm{d}s}(\xi) \times \mathbf{n}(\xi) + \mathbf{b}(\xi) \times \frac{\mathrm{d}\mathbf{t}}{\mathrm{d}s}(\xi) = \tau(\xi)\mathbf{b}(s) - \kappa(\xi)\mathbf{t}(\xi). \tag{58}$$

Collecting (53), (58), and (57) in matrix form and omitting the dependence on ξ yields

$$\begin{bmatrix} \frac{\mathrm{d}\mathbf{t}}{\mathrm{d}s} & \frac{\mathrm{d}\mathbf{n}}{\mathrm{d}s} & \frac{\mathrm{d}\mathbf{b}}{\mathrm{d}s} \end{bmatrix} = \begin{bmatrix} \mathbf{t} & \mathbf{n} & \mathbf{b} \end{bmatrix} \begin{bmatrix} 0 & -\kappa & 0 \\ \kappa & 0 & -\tau \\ 0 & \tau & 0 \end{bmatrix} = \begin{bmatrix} \mathbf{t} & \mathbf{n} & \mathbf{b} \end{bmatrix} S\left([\tau\ 0\ \kappa]^T\right). \tag{59}$$

This result corresponds to the so-called Serret-Frenet formulas, which rule the motion of $\begin{bmatrix} \mathbf{t} & \mathbf{n} & \mathbf{b} \end{bmatrix}$ along the curve. Notice that the alternative definition of curvature produces no change in these formulas.

1. A simple example

Consider the smooth sinusoidal curve given by

$$\mathbf{p}(\xi) = \begin{bmatrix} \xi & \sin(\xi) & 0 \end{bmatrix}^T, \quad \xi \in [-\pi/2, \pi/2], \tag{60}$$

which is shown in Figure 2. Simple computations show that the tangent vector $\mathbf{t}(\xi)$ and its derivative $\frac{\mathrm{d}\mathbf{t}}{\mathrm{d}s}(\xi)$ are given by

$$\mathbf{t}(\xi) = \frac{\mathrm{d}\mathbf{p}}{\mathrm{d}\xi}(\xi) \left\| \frac{\mathrm{d}\mathbf{p}}{\mathrm{d}\xi}(\xi) \right\|^{-1} = \frac{1}{(1+\cos(\xi)^2)^{1/2}} \begin{bmatrix} 1 & \cos(\xi) & 0 \end{bmatrix}^T$$

and

$$\frac{\mathrm{d}\mathbf{t}}{\mathrm{d}s}(\xi) = \frac{\mathrm{d}\mathbf{t}}{\mathrm{d}\xi}(\xi) \left\| \frac{\mathrm{d}\mathbf{p}}{\mathrm{d}\xi}(\xi) \right\|^{-1} = \frac{\sin(\xi)}{(1+\cos(\xi)^2)^2} \begin{bmatrix} \cos(\xi) & -1 & 0 \end{bmatrix}^T,$$

respectively. According to (54), the curvature can be written as

$$\kappa(\xi) = \sigma(\xi) \frac{|\sin(\xi)|}{(1+\cos(\xi)^2)^{3/2}},$$

which implies that $\kappa(\xi) = 0$ only when $\xi = 0$. Given the initial value for $\sigma(-\pi/2)$, we can conclude that

$$\mathbf{n}(\xi) = \sigma(\xi) \frac{\mathrm{sign}(\sin(\xi))}{(1+\cos(\xi)^2)^{1/2}} \begin{bmatrix} \cos(\xi) & -1 & 0 \end{bmatrix}^T, \text{ for } \xi \in [-\pi/2,\ \pi/2] \backslash \{0\}$$

and

$$\sigma(\xi) = \begin{cases} \sigma(\pi/2), & \text{for } \xi \in [-\pi/2,\ 0) \\ \sigma(0), & \text{for } \xi \in (0,\ \pi/2] \end{cases}.$$

At $\xi = 0$, we have

$$\mathbf{n}(0) = \lim_{\xi \to 0^-} \mathbf{n}(\xi) = \sigma(-\pi/2) \frac{1}{\sqrt{2}} \begin{bmatrix} -1 & 1 & 0 \end{bmatrix}^T$$

and

$$\sigma(0) = \mathbf{n}(0)^T \left(\lim_{\tau \to 0^+} \frac{\mathrm{sign}(\sin(\tau))}{(1+\cos(\tau)^2)^{1/2}} \begin{bmatrix} \cos(\tau) & -1 & 0 \end{bmatrix}^T \right) = -\sigma(-\pi/2).$$

B. Linearization of the Error Dynamics

1. *Linearization of* $\dot{\mathbf{v}}_e$

$$\frac{\partial \dot{\mathbf{v}}_e}{\partial \mathbf{v}_e}(0, \mathbf{u}_\xi, \boldsymbol{\xi}) = \frac{\partial \mathbf{f}}{\partial \mathbf{v}_B}({}^{C}_{T}R\,\mathbf{v}_r,\ {}^{C}_{T}R\,\boldsymbol{\omega}_r, \mathbf{u}_\xi) - {}^{C}_{T}R\,S(\boldsymbol{\omega}_r)\begin{bmatrix}1\\0\\0\end{bmatrix}\begin{bmatrix}1 & 0 & 0\end{bmatrix}{}^{T}_{C}R \tag{61}$$

$$\frac{\partial \dot{\mathbf{v}}_e}{\partial \boldsymbol{\omega}_e}(0, \mathbf{u}_\xi, \boldsymbol{\xi}) = \frac{\partial \mathbf{f}}{\partial \boldsymbol{\omega}_B}({}^{C}_{T}R\,\mathbf{v}_r,\ {}^{C}_{T}R\,\boldsymbol{\omega}_r, \mathbf{u}_\xi) - S({}^{C}_{T}R\,\mathbf{v}_r) \tag{62}$$

$$\frac{\partial \dot{\mathbf{v}}_e}{\partial \mathbf{d}_t}(0, \mathbf{u}_\xi, \boldsymbol{\xi}) = -V_r\kappa\,{}^{C}_{T}R\,S(\boldsymbol{\omega}_r)\begin{bmatrix}1\\0\\0\end{bmatrix}\begin{bmatrix}1 & 0\end{bmatrix} \tag{63}$$

$$\frac{\partial \dot{\mathbf{v}}_e}{\partial \boldsymbol{\lambda}_e}(0, \mathbf{u}_\xi, \boldsymbol{\xi}) = \frac{\partial \mathbf{f}}{\partial \mathbf{v}_B}({}^{C}_{T}R\ \mathbf{v}_r,\ {}^{C}_{T}R\ \boldsymbol{\omega}_r, \mathbf{u}_\xi)\,S({}^{T}_{C}R\,\mathbf{v}_r)\,Q^{-1}(\phi_C, \theta_C) \tag{64}$$

$$+\frac{\partial \mathbf{f}}{\partial \boldsymbol{\omega}_B}({}^{C}_{T}R\ \mathbf{v}_r,\ {}^{C}_{T}R\ \boldsymbol{\omega}_r, \mathbf{u}_\xi)\,S({}^{T}_{C}R\,\boldsymbol{\omega}_r)\,Q^{-1}(\phi_C, \theta_C) \tag{65}$$

$$+R_x(\phi_C)^T S(R_y(\theta_C)^T\begin{bmatrix}0\\0\\g\end{bmatrix})\begin{bmatrix}1 & 0 & 0\\0 & 1 & 0\\0 & 0 & 0\end{bmatrix} \tag{66}$$

$$\frac{\partial \dot{\mathbf{v}}_e}{\partial \mathbf{u}}(0, \mathbf{u}_\xi, \boldsymbol{\xi}) = \frac{\partial \mathbf{f}}{\partial \mathbf{u}}({}^{C}_{T}R\,\mathbf{v}_r,\ {}^{C}_{T}R\,\boldsymbol{\omega}_r, \mathbf{u}_\xi) \tag{67}$$

2. *Linearization of* $\dot{\boldsymbol{\omega}}_e$

$$\frac{\partial \dot{\boldsymbol{\omega}}_e}{\partial \mathbf{v}_e}(0, \mathbf{u}_\xi, \boldsymbol{\xi}) = \frac{\partial \mathbf{n}}{\partial \mathbf{v}_B}({}^{C}_{T}R\,\mathbf{v}_r,\ {}^{C}_{T}R\,\boldsymbol{\omega}_r, \mathbf{u}_\xi) \tag{68}$$

$$\frac{\partial \dot{\boldsymbol{\omega}}_e}{\partial \boldsymbol{\omega}_e}(0, \mathbf{u}_\xi, \boldsymbol{\xi}) = \frac{\partial \mathbf{n}}{\partial \boldsymbol{\omega}_B}({}^{C}_{T}R\,\mathbf{v}_r,\ {}^{C}_{T}R\,\boldsymbol{\omega}_r, \mathbf{u}_\xi) - S({}^{C}_{T}R\,\boldsymbol{\omega}_r) \tag{69}$$

$$\frac{\partial \dot{\boldsymbol{\omega}}_e}{\partial \mathbf{d}_t}(0, \mathbf{u}_\xi, \boldsymbol{\xi}) = 0 \tag{70}$$

$$\frac{\partial \dot{\boldsymbol{\omega}}_e}{\partial \boldsymbol{\lambda}_e}(0, \mathbf{u}_\xi, \boldsymbol{\xi}) = \frac{\partial \mathbf{n}}{\partial \mathbf{v}_B}\ S({}^{C}_{T}R\,\mathbf{v}_r)\,Q^{-1}(\phi_C, \theta_C) + \frac{\partial \mathbf{n}}{\partial \mathbf{v}_B}\ S({}^{C}_{T}R\,\boldsymbol{\omega}_r)\,Q^{-1}(\phi_C, \theta_C) \tag{71}$$

$$\frac{\partial \dot{\boldsymbol{\omega}}_e}{\partial \mathbf{u}}(0, \mathbf{u}_\xi, \boldsymbol{\xi}) = \frac{\partial \mathbf{n}}{\partial \mathbf{u}}({}^{C}_{T}R\,\mathbf{v}_r,\ {}^{C}_{T}R\,\boldsymbol{\omega}_r, \mathbf{u}_\xi) \tag{72}$$

3. Linearization of $\dot{\mathbf{d}}_t$

$$\frac{\partial \dot{\mathbf{d}}_t}{\partial \mathbf{v}_e}(0,\boldsymbol{\xi}) = \begin{bmatrix} 0 & 1 & 0 \\ 0 & 0 & 1 \end{bmatrix} \, {}^{T}_{C}R \tag{73}$$

$$\frac{\partial \dot{\mathbf{d}}_t}{\partial \boldsymbol{\omega}_e}(0,\boldsymbol{\xi}) = 0 \tag{74}$$

$$\frac{\partial \dot{\mathbf{d}}_t}{\partial \mathbf{d}_t}(0,\boldsymbol{\xi}) = V_r \, \tau \begin{bmatrix} 0 & 1 \\ -1 & 0 \end{bmatrix} \tag{75}$$

$$\frac{\partial \dot{\mathbf{d}}_t}{\partial \boldsymbol{\lambda}_e}(0,\boldsymbol{\xi}) = 0 \tag{76}$$

$$\tag{77}$$

4. Linearization of $\dot{\boldsymbol{\lambda}}_e$

$$\frac{\partial \dot{\boldsymbol{\lambda}}_e}{\partial \mathbf{v}_e}(0,\boldsymbol{\xi}) = -\text{sign}(\kappa)\sqrt{\kappa^2+\tau^2} \begin{bmatrix} 0 \\ 0 \\ 1 \end{bmatrix} \begin{bmatrix} 1 & 0 & 0 \end{bmatrix} \, {}^{T}_{C}R \tag{78}$$

$$\frac{\partial \dot{\boldsymbol{\lambda}}_e}{\partial \boldsymbol{\omega}_e}(0,\boldsymbol{\xi}) = Q(\phi_C, \theta_C) \tag{79}$$

$$\frac{\partial \dot{\boldsymbol{\lambda}}_e}{\partial \mathbf{d}_t}(0,\boldsymbol{\xi}) = -\text{sign}(\kappa) V_r \kappa \sqrt{\kappa^2+\tau^2} \begin{bmatrix} 0 \\ 0 \\ 1 \end{bmatrix} \begin{bmatrix} 1 & 0 \end{bmatrix} \tag{80}$$

$$\frac{\partial \dot{\boldsymbol{\lambda}}_e}{\partial \boldsymbol{\lambda}_e}(0,\boldsymbol{\xi}) = \begin{bmatrix} 0 & \frac{1}{\cos^2\theta_c} & 0 \\ 0 & 0 & 0 \\ 0 & \frac{\sin\theta_c}{\cos^2\theta_c} & 0 \end{bmatrix} Q(\phi_C, \theta_C) \, S({}^{C}_{T}R \, \boldsymbol{\omega}_r) \begin{bmatrix} 0 & 1 & 0 \\ 0 & 0 & 0 \\ 0 & 0 & 0 \end{bmatrix} \tag{81}$$

$$+ \, Q(\phi_C, \theta_C) \, S({}^{C}_{T}R \, \boldsymbol{\omega}_r) \, Q^{-1}(\phi_C, \theta_C) \begin{bmatrix} 0 & 0 & 0 \\ 0 & 1 & 0 \\ 0 & 0 & 1 \end{bmatrix} \tag{82}$$

Acknowledgments

This work was partially supported by Fundação para a Ciência e a Tecnologia (ISR/IST pluriannual funding) through the POS_Conhecimento Program that includes FEDER funds and by the POSI/SRI-/41938/2001 ALTICOPTER project. The work of R. Cunha was supported by a PhD Student Scholarship, SFRH/BD/5034/2001, from the Portuguese FCT POCTI program.

References

[1] Micaelli, A. and Samson, C., "Trajectory Tracking for Unicycle-Type and Two-Steering-Wheels Mobile Robots," Tech. Rep. 2097, INRIA, 1993.

[2] Kaminer, I., Pascoal, A., Hallberg, E., and Silvestre, C., "Trajectory Tracking for Autonomous Vehicles: An Integrated Approach to Guidance and Control," *AIAA Journal of Guidance, Control, and Dynamics*, Vol. 21, No. 1, 1998, pp. 29–38.

[3] Silvestre, C., Pascoal, A., and Kaminer, I., "On the Design of Gain-Scheduled Trajectory Tracking Controllers," *International Journal of Robust and Nonlinear Control*, Vol. 12, 2002, pp. 797–839.

[4] Cunha, R. and Silvestre, C., "A 3D Path-Following Velocity-Tracking Controller for Autonomous Vehicles," *16th IFAC World Congress*, Praha, Czech Republic, July 2005.

[5] Rugh, W. J. and Shamma, J. S., "Research on gain scheduling," *Automatica*, Vol. 36, 2000, pp. 1401–1425.

[6] Marcos, A. and Balas, G. J., “Development of Linear-Parameter-Varying Models for Aircraft,” *AIAA Journal of Guidance, Control, and Dynamics*, Vol. 27, No. 2, 2004, pp. 218–228.

[7] Boyd, S., Ghaoui, L. E., Feron, E., and Balakrishnan, V., *Linear Matrix Inequalities in Systems and Control Theory*, Society for Industrial and Applied Mathematics, SIAM, Philadelphia, PA, 1994.

[8] Tomizuka, M., “Optimum Linear Preview Control with Application to Vehicle Suspension-Revisited,” *American Society of Mechanical Engineers - Journal of Dynamic Systems, Measurement, and Control*, Vol. 98, No. 3, 1976, pp. 309–315.

[9] Prokop, G. and Sharp, R. S., “Performance enhancement of limited bandwith active automotive suspensions by road preview,” *Institution of Electrical Engineers Proceedings - Control Theory and Applications*, Vol. 142, No. 2, 1995, pp. 140–148.

[10] Takaba, K., “Robust servomechanism with preview action for polytopic uncertain systems,” *International Journal of Robust Nonlinear Control*, Vol. 10, 2000, pp. 101–111.

[11] Paulino, N., Silvestre, C., and Cunha, R., “Affine Parameter-Dependent Preview Control for Rotorcraft Terrain Following Flight,” *AIAA Journal of Guidance, Control, and Dynamics*, 2006, accepted for publication.

[12] Craig, J. J., *Introduction to Robotics and Control: Mechanics and Control, 2nd ed.*, Addison-Wesley Publishing Company, Massachusetts, 1989.

[13] Scherer, C. and Weiland, S., *Lecture Notes on Linear Matrix Inequalities in Control*, Dutch Institute of Systems and Control, 2000.

[14] Ghaoui, L. E. and Niculescu, S. I., editors, *Advances in Linear Matrix Inequality Methods in Control*, Society for Industrial and Applied Mathematics, SIAM, Philadelphia, PA, 1999.

[15] Paulino, N., Silvestre, C., and Cunha, R., “Terrain Following Controller for Affine Parameter-Dependent Systems: An Application to Model-Scale Helicopters,” *AIAA Guidance, Navigation, and Control Conference*, San Francisco, CA, Aug. 2005.

[16] Cunha, R. and Silvestre, C., “Dynamic Modeling and Stability Analysis of Model-Scale Helicopters with Bell-Hiller Stabilizing Bar,” *AIAA Guidance, Navigation, and Control Conference*, Austin, TX, Aug. 2003.

[17] Kaminer, I., Pascoal, A., Khargonekar, P., and Coleman, E., “A Velocity Algorithm for the Implementation of Gain-Scheduled Controllers,” *Automatica*, Vol. 31, No. 8, 1995, pp. 1185–1191.

[18] Cunha, R. and Silvestre, C., “*SimModHeli*: A Dynamic Simulator for Model-Scale Helicopters,” *11th Mediterranean Conference on Control and Automation MED’03*, Rhodes, June 2003.